Jérémy MAYEN

Master's degree 2 internship report: Chemistry and Life Sciences, speciality Molecular Biology and Environmental Microbiology

Spatial and temporal variations in pCO_2 and atmospheric CO_2 exchanges in a temperate salt marsh system

French research institute for exploitation of the sea (IFREMER)

Resources and Environment Laboratory of the Pertuis Charentais (LER-PC)

Internship supervisor: Pierre POLSENAERE

"This report is an educational exercise that can in no way engage the responsibility of the host laboratory".

Ifremer institute presentation

The French research institute for exploitation of the sea (Ifremer) was created in 1984 by the fusion of the national centre for ocean development and the scientific and technical institute of marine fisheries. Nowadays, with a staff of 1500 researchers, engineers and technicians and a budget of around 240 million euros, Ifremer is the French reference institute for knowledge of the marine environment and its resources. It is composed of 23 research units organised in 4 different scientific departments: (i) Biological Resources and Environment, (ii) Physical Resources and Seabed Ecosystems, (iii) Oceanography and Ecosystem Dynamics and (iiii) Research Infrastructures and Information Systems. Present on all of France's coastlines and overseas territories, Ifremer laboratories are located in the three major oceans: the Indian Ocean, the Atlantic Ocean and the Pacific Ocean. In addition to the monitoring of the marine and coastal environment, the Ifremer lead several research projects in marine sciences, from the coastal zone to the deep seabed with national, European and global collaborations. Indeed, 510 scientific papers were published in 2017 by Ifremer according to Web of Science.

The Resources and Environment Laboratory of the Pertuis Charentais (LER-PC) at the La Tremblade station is one of the nine coastal laboratories of the "Littoral" Unit. This unit is part of the Oceanography and Ecosystem Dynamics department which focuses its activities on the observation, modelling and understanding of the physical ocean at different scales, as well as pelagic and benthic coastal ecosystems. The main mission of the Ifremer lab LER-PC is to lead research projects on biogeochemical processes and nutrients fluxes at the terrestrial – aquatic – atmospheric interfaces in the coastal zone. For instance, the Aiguillon project (2017-2020) allowed better understanding carbon and nutrients (N, P, Si) dynamics in the different water masses along the Poitevin marshes – Aiguillon Bay – Breton Sound. The ANR-PAMPAS project (2019-2022) focuses on carbon dynamics and associated atmospheric fluxes in relation to abiotic and biotic environmental parameters at the temporal scale within different temperate marsh systems. Moreover, LER-PC research projects are also related to the evolution and adaptation of water column microbial communities to environmental variability in coastal ecosystems. To finish, LER-PC is involved in several coastal zone observation and monitoring networks such as REPHY that identify species of phytoplankton and phytotoxins in Charentais Sounds and REMI, the network for the microbiological control of shellfish farming.

Acknowledgements

I would like to thank Audrey Bruneau, supervisor of the Ifremer lab LER-PC and Bénédicte Charrier, supervisor of the Ifremer station at La Tremblade for their warm welcome at the laboratory and for allowing me to complete this internship.

I would like to thank Pierre Polsenaere very warmly and sincerely for trusting me again for this Master's degree internship. Thank you very much for leading me with such kindness. Thank you also for giving me the opportunity to perform these oral presentations of the research project to partners such as the Lilleau des Niges nature reserve and the LIENSs at the La Rochelle University. It was really formative for me to work together, both in terms of studying carbon dynamics in coastal areas and in terms of research, thank you again!

Many thanks to Philippe Geairon for our field trips to Le Fier d'Ars, Marans and Genouillé. Thank you for your help during the filtrations in the truck, without the help of your wrist, I wouldn't have been able to do it on my own. Thank you for all the good times we had. I would like to warmly thank Jean Michel Chabirand for guiding me in metrology and phytoplankton reading. Thank you for our long discussions in the car. Enjoy your retirement Jean-Mi, you have well deserved it.

I would like to thank Jonathan Deborde for his help and his very useful advices but also for his good mood.

Thanks to Elise Coignot and Hugo Gerveais for their help but also for all these good moments.

Thanks to James Grizon for taking me out to sea, it is been a pleasure.

I would like to thank all the laboratory staff for their warm welcome without forgetting Joelle, Isabelle and Anne.

Finally, a big thank you to the carsharing team (Anne, Pierre, James, Bénédicte, Elise and Jean-Mi) without which the 140 km per day would have been much more complicated.

Table of Contents

Introduction

Coastal environments such as the Charentais Sounds are key systems in the biogeochemical cycle coupling (C, N, S) between land, ocean and atmosphere. They carry large quantities of carbon between (i) the drainage basin and the ocean (horizontal transport) and (ii) the water column and the atmosphere or sediments (vertical transport). Within the coastal zone, wetlands represent exceptional ecosystems from an ecological point of view. Firstly, they have a strong biodiversity including terrestrial and aquatic vegetations, migratory birds, freshwater and saltwater fish, phytoplankton, mesoplankton and bacteria. In addition to this habitat function, these highly productive coastal environments also perform others ecosystems functions such as the hydrologic functioning allowing the water cycle regulation and the biogeochemical function permitting the natural water purification. The Charentais Sound marshes are the support for many economic activities such as the salt-, oyster- and fish-farming, and have a strong heritage identity due to their sites, their remarkable landscapes and their role as a refuge for biodiversity. However due to the tidal influence, these marshes are exposed to sea level rise and marine submersion but also to global changes in general including anthropogenic pressures such as water acidification or increased organic carbon inputs from the land.

Carbon dynamic studies within the coastal wetlands and particularly in salt marshes are relatively recent and few nowadays. It is therefore important to precisely study what are the different factors influencing carbon processes and fluxes at the different terrestrial-aquatic-atmospheric exchange interfaces in these dynamic ecosystems and at the different temporal scales. This thematic is developed by the Ifremer lab LER-PC in the ANR-PAMPAS project (2019-2022) supported by the LIENSs at the La Rochelle University. The project allows a better understanding of marsh functioning located in the Charentais Sounds according to management practices through the characterization of their heritage identity evolution faced with the risks of oceanic submersion. Built on collective and participatory research and engineering approaches, this research project allows for the crossing of expertise in Human and Social Sciences, Life and Earth Sciences and that one of the marshland managers (consortium of 72 people). Through this Master's degree training period, pCO_2 and water-atmosphere CO_2 fluxes have been studied within a temperate salt marsh system on the Ré island (France) at the temporal and spatial scale to (i) study the different factors controlling this dynamic and ecosystem metabolisms and (ii) better understand their role in regional and global carbon cycles.

1. State of the Art

1.1. Place and problematic of the coastal zone in global carbon budget

1.1.1.1. The global carbon cycle

On Earth, the global carbon cycle is defined as a whole of reservoirs (land, ocean, atmosphere) in equilibrium and interconnected by natural carbon (C) flows allowing ecosystem biogeochemical functionning (Ciais et *al.*, 2013). Before the industrial area, carbon dioxide (CO_2) was exchanged between the atmosphere and land, ocean reservoirs up to 120 and 90 $GtC.yr^{-1}$ respectively (Figure 1) involving only chemicophysical and biological processes (solubility pump, respiration of living beings and photosynthesis of autotrophic organisms) (Prentice et *al.*, 2011). However, since the 17th century, anthropogenic activities have significantly modified this natural balance of the global carbon budget by releasing large quantities of CO_2 into the atmosphere (11.0 ± 0.8 $GtC.yr^{-1}$) mainly by burning of fossil fuel (E_{PP}, 86%) and by the land use change such as deforestation (E_{LUC}, 14%) (Friedlingstein et *al.*, 2019) (Figure 1). Consequently, atmospheric CO_2 exchanges with terretrial biosphere and ocean were increased of ~ 11% and ~ 34% respectively (Friedlingstein et *al.*, 2019) (Figure 1). At the same time, atmospheric CO_2 concentration increased from 280 ppm (part per million) in 1750, to 367 ppm in 1999 (Prentice et *al.*, 2011), to reach 414 ppm in February 2020 according

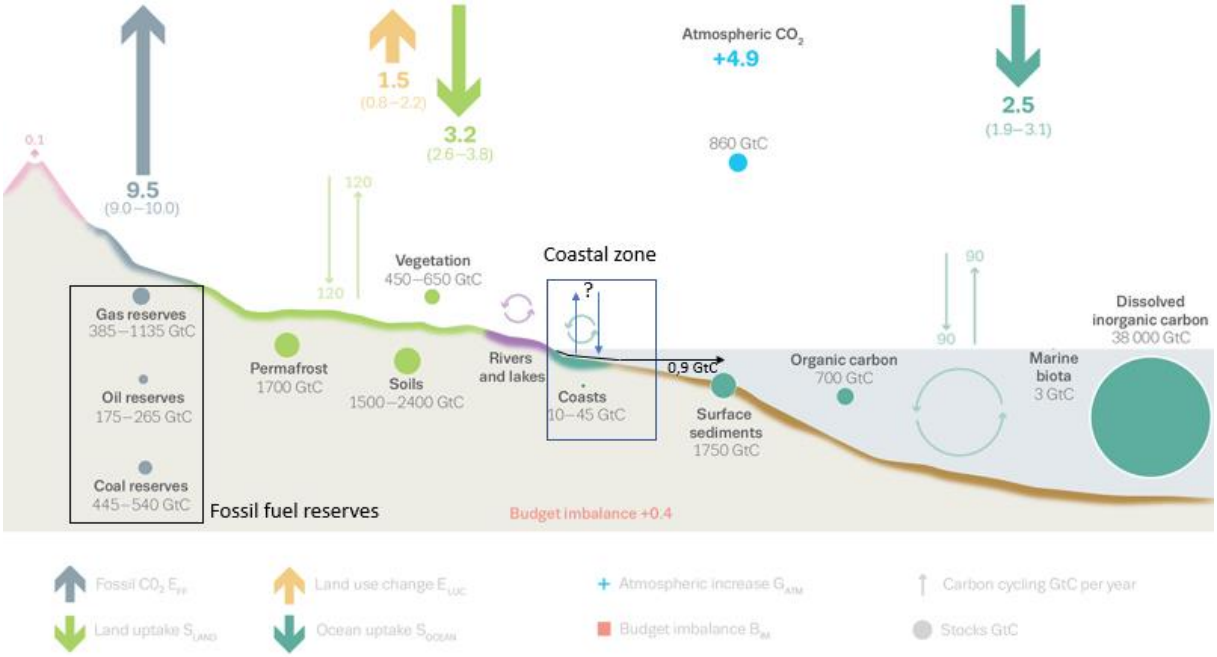

Figure 1: Global carbon cycle for the decade 2009-2018 (modified from Friedlingstein et *al.*, 2019). Carbon stocks are represented in Giga tons of Carbon (1GtC = 10^{15}g). The natural and anthropogenic fluxes are represented in Giga tons of Carbon per year ($GtC.yr^{-1}$). The main anthropogenic C fluxes are fossil CO_2 emissions (E_{FF}) and land use change emissions (E_{LUC}).

to the National Oceanic and Atmospheric Administration (NOAA, 2020). The CO_2 is a greenhouse gas (GHG) that absorbs infrared radiations emitted from the earth's surface (Environmental Protection Agency, EPA). Thus, anthropogenic increases in GHG concentrations are the origin of climate changes such as atmospheric and oceanic warming, sea level rise, increase in extreme events or ocean acidification (Bindoff et *al.*, 2013). It is therefore important to study the redistribution of anthropogenic CO_2 emissions and their influence on C processes in all compartments and particularly in the coastal zone which is a major interface system between ocean, land and atmosphere.

1.1.2. The coastal zone, a dynamic and heterogeneous interface

The coastal zone is defined as the oceanic area located on the continental shelf with an average depth of less than 200 meters, including all the estuarine surface up to the upstream limit of the tidal influence (Polsenaere, 2011). Despite their small surface area (only 7% of the global ocean), the coastal area carries out major ecological functions such as primary production (14 to 30 % of total ocean primary production), bacterial mineralization, organic matter burial and the deposition of the calcium carbonate (Gattuso et *al.*, 1998). Constituted both of terrestrial, oceanic and brackish waters, it has a wide diversity of geomorphological types and ecosystems (shelves, estuaries, fjords, wetlands, rivers) allowing the biogeochemical cycle coupling (C, N, P, S, Si) between land, ocean and atmosphere (Aufdenkampe et *al.*, 2011; Bauer et *al.*, 2013). On the one hand, these dynamic and heterogeneous ecosystems behave as an active horizontal pipe carrying and processing large quantities of nutrients and carbon (~0.90 ± 0.05 $GtC.yr^{-1}$) between the drainage basin and the open ocean (Cai, 2011; Cole et *al.*, 2007) (Figure 1). When they are in excess, these terrestrial inputs can cause eutrophication problems in coastal environments leading to anoxic and hypoxic areas (Howarth et *al.*, 2011). On the other hand, the coastal zone also exchanges vertically significant and variable quantities of C both with the atmosphere and the sediments (Cole et *al.*, 2007; Najjar et *al.*, 2018). At the global scale, wetlands and shelves absorb from the atmosphere -0.55 ± 0.05 and -0.25 ± 0.05 $PgC.yr^{-1}$ respectively whereas, estuaries emit +0.25 ± 0.05 $PgC.yr^{-1}$ to the atmosphere (Bauer et *al.*, 2013) (Figure 2). Contrary to CO_2 supersaturated estuarine waters due to a strong bacterial mineralization activity (Frankignoulle et *al.*, 1998), other coastal environments such as the wetlands and particularly, salt marshes are key zones in atmospheric C fixation by primary producer activity (vegetation, phytoplankton and microphytobenthos) (Bauer et *al.*, 2013). The organic carbon (OC) part produced through photosynthesis can largely be sequestered and

stored as “the blue carbon” in the sediments of theses vegetated coastal ecosystems (Mcleod et *al.*, 2011) that in turn strongly contribute to the global carbon cycle (Friedlingstein et *al.*, 2019). Strong heterogeneity is also observed in these systems at characteristic temporal scales (diurnal, tidal, seasonal and annual). It complicates the integrative approach of spatial and temporal variations in C processes and fluxes in and between compartments and thus requests further measurements (Cai, 2011; Najjar et *al.*, 2018).

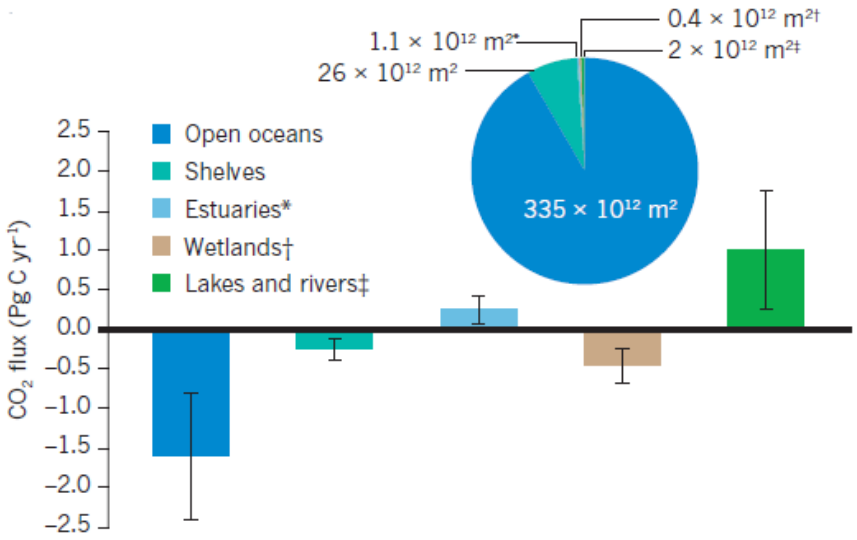

Figure 2: Global atmosphere-water CO_2 fluxes ($PgC.yr^{-1}$) in different aquatic ecosystems of the coastal zone (Bauer et *al.*, 2013). 1PgC = 1GtC = 10^{15}g.

1.1.3. Coastal carbon biogeochemistry

Carbon in coastal waters supplying salt marshes through horizontally advection may be present in both organic (44.5%) or inorganic (55.5%) forms, particulate (> 0.45 µm) or dissolved (< 0.45 µm) (Aminot and Kérouel, 2004; Cai, 2011). The particulate organic carbon (POC, 20.8%) may be either brought by rivers and have an allochthonous origin (drainage basin erosion) or produced inside the ecosystems (autochthonous origin) by terrestrial plant or phytoplanktonic, macroalgae and seagrass primary productions. In the ocean, the POC is mainly of phytoplankton origin, whereas in coastal environments and in particular in estuaries, the land-based contribution from rivers frequently predominates when flows are high in winter and the turbidity slows the phytoplanktonic growth. On the contrary, in summer at low water level, POC may be produced by a strong freshwater phytoplanktonic activity brought by rivers and moreover, degraded in the estuary (Aminot and Kérouel, 2004). The dissolved organic carbon (DOC, 23.7%) form can derive either from the terrestrial humus inputs or from the microbial

degradation of phytoplankton (He et *al.*, 2010). The dissolved inorganic carbon (DIC, 39.2%) form in the coastal environments includes three different forms: the carbon dioxide (CO_2, ~ 1%), carbonate (HCO_3^-, ~ 91%) and bicarbonate (CO_3^{2-}, ~ 8%) ions (Ciais et *al.*, 2013). The DIC can be originated either from the food web respiration or from benthos-pelagos exchanges but also be brought by freshwater from drainage basin. These ions contribute to the water's buffering capacity (alkalinity), limiting pH decreases in oceanic and coastal water masses linked to CO_2 increase (Denman et *al.*, 2007).

1.2. Coastal marshes among wetlands

1.2.1. Wetlands: exceptional but threatened ecosystems

Wetlands are "areas of marsh, fen, peatlands or water, whether natural or artificial, permanent or temporary with water that is static or flowing, fresh, brackish or salt, including areas of marine water the depth of which at low tide does not exceed six metres" (An Introduction to the Convention on Wetlands). As an integral part of the coastal zone, these exceptional ecosystems are very heterogeneous from a morphological and ecological point of view. For example, in the Nouvelle Aquitaine region of France, wetlands covering between 12.50 and 18.75% of soil within 500 meters of the Atlantic Ocean, are present in various forms of coastal marshes, lakes and ponds, lagoons and estuaries, peatlands, alluvial valley bottoms and headwater wetlands (AcclimaTerra, 2018).

These interface zones between the terrestrial and aquatic domains perform several functions of water cycle regulation (hydrologic function) and habitats for a characteristic flora and fauna. They are also considered as natural filters (biogeochemical function) because these ecosystems allow mineral and organic matter removal by vegetation and microorganism activity (AcclimaTerra, 2018; Tortajada, 2011). Actually, the microbial activity of fungi in salt marshes can remove up to 60% of the aboveground organic matter (Newell and Porter, 2020). Then, a refractory part of the POC can be storage as "blue carbon" in the mudflat sediments of the seagrass coastal wetlands (Berg et *al.*, 2019; Mcleod et *al.*, 2011). Several studies have shown that coastal wetlands have high C stocks in their sediments (Chow et *al.*, 2013) and are therefore critical elements of global carbon budget (Najjar et *al.*, 2018). According to the Intergovernmental Panel on Climate Change, the C stock of wetlands is 240 GtC for 0.35×10^9 ha (Watson et *al.*, 2000). However, despite their major ecological potential, wetlands are the most threatened ecosystems on the Earth by global changes such as the sea level increase, the

continuous conversion and pollution but also the overexploitation of their resources (An Introduction to the Convention on Wetlands). Salt marshes have globally lost 25% of their surface since 1800s at an annual rate of 1-2% (Mcleod et *al.*, 2011). Their importance as ecosystem service reservoirs has allowed the implementation of protection and conservation policies that contribute to their better management and to the maintenance and development of their ecological and economic potentials (AcclimaTerra, 2018).

1.2.2. Salts marshes characteristics

Among wetlands, marshes are characterised by shallow stretches of water, often close to waterways, estuaries or the sea and with herbaceous vegetation that is adapted to saturated soil conditions. These biodiversity reservoirs in terms of fauna, flora and microorganisms (cyanobacteria) are intermittently or continually inundated with water (EPA; Tortajada, 2011). Marshes may be classified depending on the water salinity ($S < 3$: freshwater, $3 < S < 15$: brackish water and $S > 15$: saltwater) or the influence of the tide (tidal and non-tidal) according to EPA. Only two different types of marshes are present on the French Atlantic coast, the freshwater and the saltwater marshes (AcclimaTerra, 2018). Floods of adjacent rivers and lakes can largely influence freshwater marshes whose the most frequent plant species include a number of grasses, sedges and rushes with an important presence of herbaceous vegetation (mainly *Pontedaria* and *Sagittaria*) (Craft, 2016). Salt marshes are defined as "coastal wetlands that are flooded and drained by the salt water brought in by the tides" with a soil composed of deep mud and peat (NOAA, 2020).

Salt marshes include two distinct areas called respectively the slikke and the schorre and are characterized by different submersion frequencies of coastal waters (Figure 3). Firstly, the slikke is the lower and middle parts of the intertidal zone made up of muddy sediments and large channels that are flooded at each high tide, even during neap tides. It is poorly vegetated, except for the highest part covered with marine phanerogams, especially the *Zostera noltii* specie. Furthermore, the slikke is also the place of a significant microphytobenthos development that migrates at the surface at low tide to perform the photosynthesis and then, return in the mudflat during the high tide. For instance, a study on the Charentais Sounds has showed a microphytobenthic primary production of 60.8 $gC.m^{-2}.yr^{-1}$ in a temperate intertidal mudflat (Savelli et *al.*, 2019). Made up of photosynthetic benthic microalgae (diatoms, cyanobacteria, euglenophyta, chlorophyta) (Honeywill et *al.*, 2002), the microphytobenthos

activity is mainly controlled by abiotic factors such as the mudflat characteristic and temperature, the photosynthetically active radiation (PAR) and the tidal power (Savelli et *al.*, 2019). Then, the schorre corresponds to the highest levels of salt marshes, directly connected to the terrestrial environment and covered by saltwaters only during spring tides (high tide coefficients). Vegetation (*Salicornia obscura* and *Spartina maritima*) slows down the tidal power and contributes to the sedimentation of the suspended solids present in the water (Oustin, 2003). At last, some parts of the schorre within the French coastal zone have been closed (dykes) giving way to other types of salt marshes (Champion et *al.*, 2012). Nowadays, theses dyked salt marshes (Paticat, 2007) have different management practices according to socio-economic and cultural activities; for instance they are either protected within a natural reserve to conserve their many ecosystem functions or used for-profit human activities as salt-, oyster- and fish-farming (Bel Hassen, 2000). The functioning of these salt marshes can be controlled by two mechanisms: (i) the tidal influence allowing resuspension of both OC in sludge and microphytobenthos on the intertidal mudflat (slikke); and (ii) water renewal according to activity type within salt marshes that can enrich drainage channels either in nutrients (fish-farming) or in fresh materials (oyster-farming) (Tortajada, 2011).

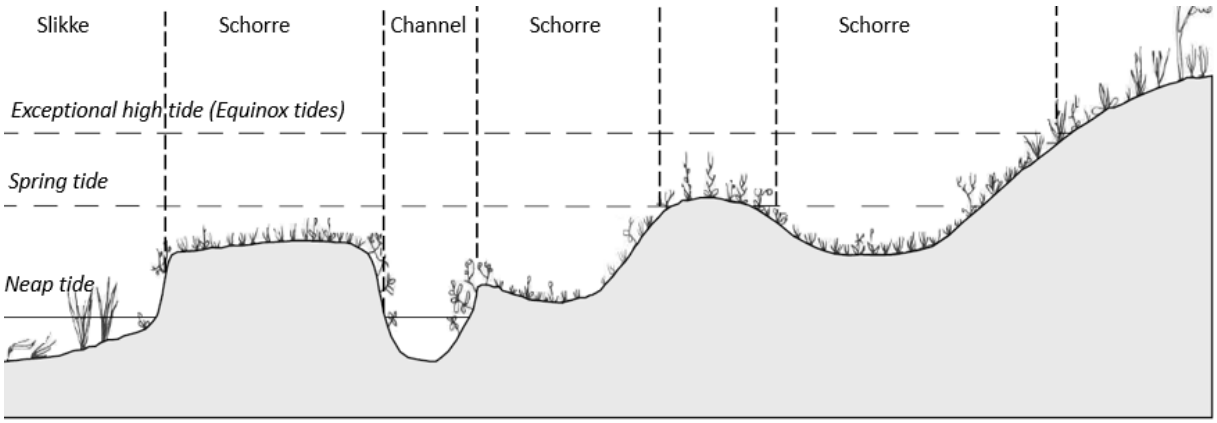

Figure 3: Intertidal zone classification (modified from Paticat, 2007).

1.3. Salt marsh metabolism

1.3.1. Definitions, processes and environmental controlling factors

Metabolism or more precisely, the net ecosystem production (NEP) is a key concept in the carbon dynamic and budget research studies. This term describes the ability of the terrestrial and aquatic ecosystems to consume inorganic carbon (CO_2) to produce OC by the autotrophic organism activity (plants and microorganisms) (Chapin et *al.*, 2006). NEP is thus define as (i)

the difference between the ecosystem-level gross primary production (GPP) and community respiration (CR) and as (ii) the net carbon accumulation in the ecosystem (Gattuso et *al.*, 1998; Woodwell and Whittaker, 1968). It allows thus to describe the ecological state of the ecosystems (NEP > 0: autotrophic system and NEP < 0: heterotrophic system). Generally, net autotrophic ecosystems import inorganic nutrients and DIC (CO_2) and export or bury OC in the sediments whereas, the net heterotrophic ecosystems import OC and export nutrients and DIC (Crosswell et *al.*, 2017; Nixon et *al.*, 1995).

Since several years, biogeochemical studies have showed that salt marshes are autotrophic systems with a positive NEP in contrast to estuaries (Fagherazzi et *al.*, 2013; Najjar et *al.*, 2018; Weston et *al.*, 2014). Owing to strong photosynthesis activity rates of primary producers (terrestrial plants, aquatic algae and seagrasses), these highly productive coastal ecosystems appear thus nowadays as atmospheric CO_2 sink (Schäfer et *al.*, 2014). Two different metabolic pathways are particularly involved. First, the photo-autotrophy of the vegetation and the phytoplankton using light energy to CO_2 fixation (photosynthesis), has rates of NPP ranging from 100 to > 2500 $gC.m^{-2}.yr^{-1}$ (Tobias and Neubauer, 2019) with highest values in the south Atlantic and gulf Coast salt marshes (Mendelssohn and Morris, 2002). Moreover, the chemoautotrophy of autotrophic microorganisms has also a significant contribution to the marsh NPP by converting the CO_2 in OC with the chemical energy. For example, sulfur-mediated chemoautotrophy process ranges from 20 to 480 $gC.m^{-2}.yr^{-1}$ and Fe(II)-oxidizing bacteria (FeOB) activity allows lower NPP rates from 2 to 185 $gC.m^{-2}.yr^{-1}$ (Tobias and Neubauer, 2019). With regards to OC mineralization by the biological pump, the aerobic respiration account for 18 to 30% of the total salt marsh respiration (Furukawa et *al.*, 2005).

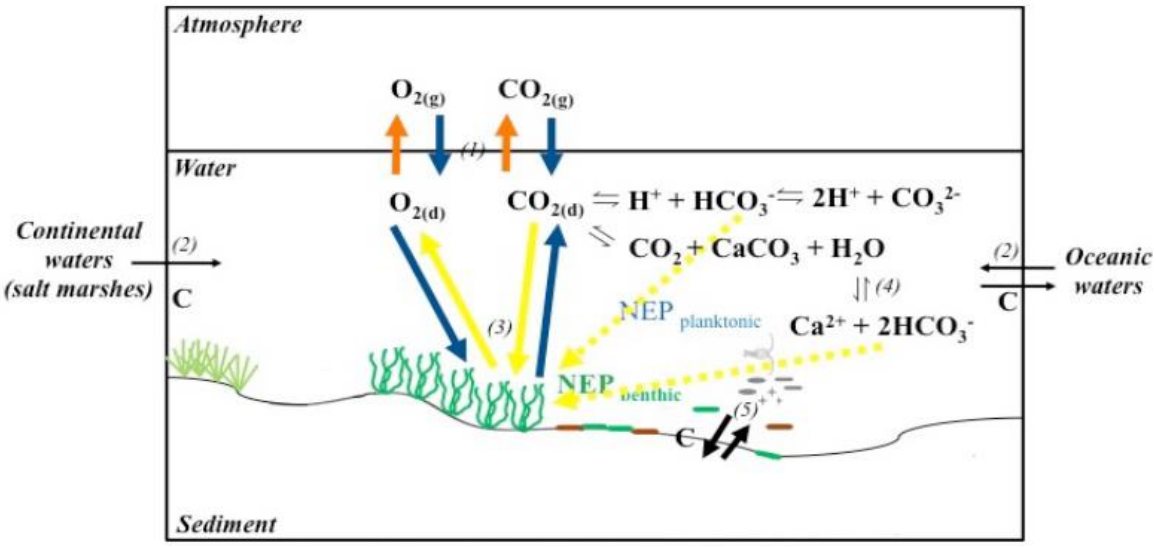

Figure 4: Different processes influencing the C dynamic in coastal zone (Polsenaere, 2011).

Carbon and atmospheric CO_2 flux dynamics in the coastal area and especially in salt marshes are influenced by several chemicophysical and biological processes between the different compartments of the ecosystem and depending on diurnal, tidal, seasonal and annual time scales (Figure 4). Carbon exchanges are thus controlled by (1 in Figure 4) the chemicophysical pumps allowing to master CO_2 fluxes with the atmosphere (absorption or degassing) according to the water temperature (Denman et *al.*, 2007) and the water CO_2 concentration. More precisely, when partial pressures of CO_2 (pCO_2) in water are lower than atmospheric pCO_2 (414 ppm), salt waters are thus undersaturated and the chemical pump permits to absorb CO_2 in the salt marsh waters and in return; (3 in Figure 4) the biological pump controlled by photosynthetic activity of the vegetation and autotrophic microorganisms (benthic and pelagic) but also by the food web respiration. Therefore, the POC fraction that is not mineralized at the surface by microorganisms (refractory carbon) is transferred at depth by the biological pump; (4 in Figure 4) the carbonate counter pump allowing the formation and the release of CO_2 by the calcium carbonate ($CaCO_3$) precipitation (calcification). On the contrary, the dissolution of the calcium carbonate constitutes a CO_2 sink and could have a major contribution in the global carbon budget by $CaCO_3$ burial (Macreadie et *al.*, 2017); (5 in Figure 4) the benthos-pelagos exchanges which control the OC burial in the sediments including the "blue carbon" largely sequestered in salt marshes (Artigas et *al.*, 2015; Juppin, 2018; Najjar et *al.*, 2018). Indeed, their major role in the carbon storage on Earth is known with an average soil carbon density of 0.039 ± 0.003 $g.cm^{-3}$ (Chmura et *al.*, 2003) and an average soil carbon sequestration rate of 218 ± 24 $g.m^{-2}.yr^{-1}$ (Mcleod et *al.*, 2011). Finally, horizontal advection processes (2 in Figure 4) also significantly influence the salt marsh carbon cycling with on the one hand, terrestrial carbon inputs from the drainage basin and on the other hand, open or coastal ocean exchanges (Najjar et *al.*, 2018).

To illustrate, Wang et *al.* (2016) through continuous *in situ* measurements of relevant biogeochemical (carbon) parameters and water fluxes in an intertidal salt marsh of the U.S. northeast region estimated a total net CO_2 fixation (NPP) of 13.2 $TgC.yr^{-1}$. On this total NPP value, 56% were exported to the coastal ocean (inorganic and organic carbon representing 39 and 17% respectively) meaning that marsh tidal C (DIC) export could represent a major term (414 $g.C.m^{-2}.yr^{-1}$) in the marsh carbon budget. The remaining part of this total NPP were split between CO_2 degassing to the atmosphere and OC burial ("blue carbon") with 34 and 11% respectively representing significant fluxes in this budget too (Wang et *al.*, 2016).

1.3.2. Salt marsh carbon process and flux methodological approaches

The strong heterogeneity in C biogeochemical processes within coastal wetlands at spatial and temporal scales (Schäfer et *al.*, 2014; Weston et *al.*, 2014) need integrative C process and exchange measurements between all compartments (Figure 4) over times to better understand the ecological functioning of theses ecosystems facing global changes. In some ecological studies, autonomous underwater probes are used for high-frequency measurements of water pCO_2 allowing then to study *in situ* CO_2 dynamics in relation to other processes such as benthic metabolisms at the diurnal, tidal and seasonal scales. For example, Berg et *al.* (2019) have shown that pCO_2 values in a seagrass meadow (Virgina, U.S.) were ranged between 193 and 859 ppmv in spring with a strong control of these diurnal fluctuations by the seagrass metabolism. From these measured water pCO_2, water-air CO_2 fluxes can be estimated by Takahashi et *al.* (2002) whose the formula takes into account both CO_2 gas transfer velocity, the CO_2 solubility in water and the water-air pCO_2 difference. With this methods, Coignot et *al.* (2020) have showed for instance that the Poitevin marsh degassed large quantities of CO_2 to the atmosphere linked to bacterial mineralization contrary to protected salt marshes of Fier d'Ars (France) which behave as a CO_2 sink in spring (Mayen, 2019). Regarding the benthos-pelagos exchanges, a tidal marsh study in the southeastern U.S. has allowed to quantify the DIC exchanges between the sediment and the water column by using the benthic chamber incubations (Cai et *al.*, 1999). Floating chambers can be used to measure *in situ* CO_2 fluxes at the water-air interface (Abril et *al.*, 2009; Guérin et *al.*, 2007) but this invasive method may increase the turbulence at the water surface when the wind speed is low (Polsenaere et *al.*, 2013). Others studies have implemented the Eddy Covariance (EC) methods over intertidal flats or in salt marshes to measure *in situ* CO_2 fluxes at the mudflat-air and saltwater-air interfaces. This innovative and non-intrusive method shows nowadays a growing interest to study the metabolism of these coastal ecosystems under true field conditions and to integrate them into regional C budgets (Polsenaere et *al.*, 2012).

1.4. Internship objectives

The Littoral Unit of Ifremer funded this internship linked to the ANR-PAMPAS and takes place at the LER-PC. Regarding the natural dimension of this heritage identity of the Charentais Sounds marshes, the laboratory focuses on C dynamics and particularly on water pCO_2 variations and associated atmospheric fluxes in relation to abiotic and biotic environmental parameters at the different time scales. The purpose is to better understand the biogeochemical

functioning of these coastal areas and *in fine*, their role in regional and global carbon cycles. Through an approach mixing *in situ* measurements/sampling of relevant environmental and biogeochemical parameters by different autonomous probes and laboratory analysis, this training period has allowed to study precisely water pCO_2 and water-air CO_2 exchanges and associated controlling factors within a sound-bay-salt marsh continuum at the diurnal, tidal and seasonal scales. Moreover, *in situ* and *in vivo* measurements of chlorophyll *a* concentrations were performed to follow the phytoplankton biomass at the same time scale. The different sites choose for this internship are connected to coastal waters through the Fier d'Ars Bay and are associated to different salt marsh areas and management practices on Ré Island (intertidal bay, channel, dyked salt marsh).

2. Materials and methods

2.1. Study sites

Within the French Atlantic Ocean, the Fier d'Ars is a 750-hectare (ha) internal bay located at the North of the Ré Island and connected to the Breton Sound through a 700-metre wide opening (Figures 5 and 6). It corresponds to an intertidal system since at each tide, the Fier d'Ars is alternately submerged and emerged by coastal waters revealing the intertidal mudflat twice a day (Bel Hassen, 2001). Moreover, this inland sea has a coastal marsh and mudflat complex (1 200 ha) with salt-, oyster- and fish-farming activities mainly on the foreshore and

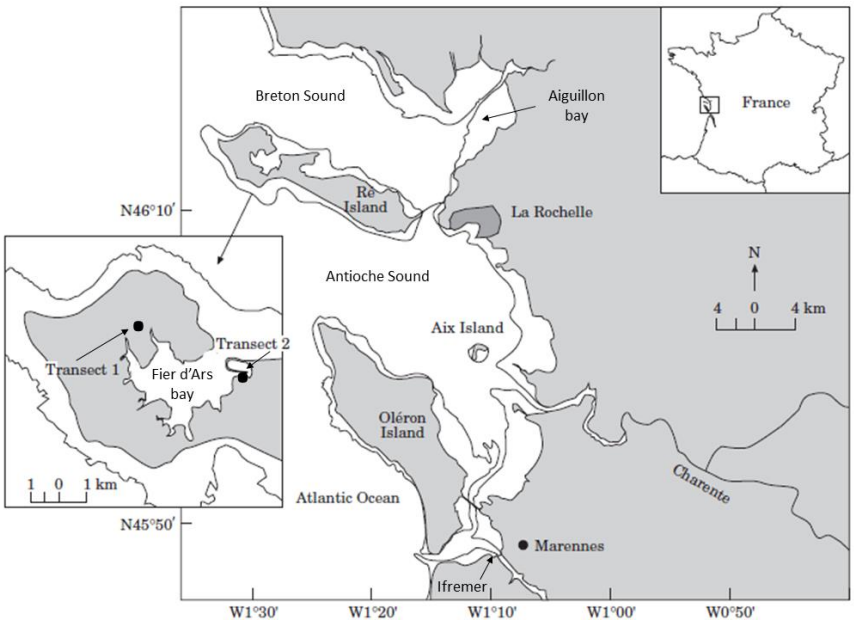

Figure 5: Geography of the Fier d'Ars Bay on the Ré Island in France and the location of the two study dyked salt marshes (Transect 1: A1 marsh; Transect 2: Loix marsh) (modified from Bel Hassen, 2001).

in the dyked salt marshes (Bel Hassen, 2000; Weiss, 1997) (Figure 6). Since 1981, a part of this coastal wetland is protected within the Lilleau des Niges National Natural Reserve (NNR, 190 ha) that allows strengthening favourable environments for the nesting and wintering of birds (Champion et *al.*, 2012). Indeed, the Fier d'Ars has a high biodiversity with an exceptional migratory bird number but also a vegetation of 168 species of vascular phanerogams and cryptogams (*Ruppia maritima* and *cirrhosa* in salt marshes, *Zostera noltei* on mudflats and *Limonium auriculiursifolium* as a terrestrial plant species). These terrestrial and aquatic plants constitute the main primary producers of the Fier d'Ars with the aquatic macroalgae and the phytoplanktonic and microphytobenthic communities (Champion et *al.*, 2012).

Figure 6: Locations of the four study sites within the Sound-intertidal bay-salt marsh continuum: Fier d'Ars bay (station *a*), Vieux Port channel (station *b*), A1 marsh (station *c*) and Loix marsh (station *d*).

The different water samplings and *in situ* measurements within this coastal wetland were perform seasonally from March 2018 to February 2020 at four interconnected stations (*a*, *b*, *c* and *d*, Figure 6) along a Sound-intertidal bay-coastal marsh continuum through two research projects: (i) PAMPANINO in 2018 with the stations *a* and *b* (Fier d'Ars Bay and Vieux Port channel respectively, Figure 6) and (ii) the RNA-PAMPAS project (from 2019 to 2020) associated with the study of two "vasais" of the Fier d'Ars which have different management practices and configurations (stations *c* and *d* respectively, Figure 6) (Table S1). Vasais are dyked salt marshes (~0.5 metre deep) permitting to store saltwater during the neap tide periods in summer and then to supply the downstream marshes by gravitation (Champion et *al.*, 2012).

The A1 marsh (station *c*, Figure 6) in the NNR is a low anthropized salt marsh supplied in coastal waters indirectly by the Vieux Port channel (station *b*, Figure 6) through a lock. During winter, at each black moon when tidal coefficients are higher than 70, the lock is left open. From spring to autumn, the lock is permanently open to find the best compromise between salt- and fresh- mixing waters to promote both *Ruppia maritima* seagrass development in the marsh and the eel passage from Sound waters to the marsh (Champion et *al.*, 2012). Then, the second studied marsh located at the Loix ecomuseum vasais (station *d*, Figure 6) is directly connected to coastal waters of the Fier d'Ars Bay (station *a*) by a lock whose management practice depends on downstream salt-farming activity.

2.2. Probes and measurement strategies

Sub-surface water (20 cm below the surface) CO_2 partial pressures (pCO_2) and other biogeochemical parameters were measured once per minute autonomously during 24-hour cycles at stations *a*, *b*, *c* and *d* (Figure 6) at each season (Table S1) to catch relevant temporal (diurnal, tidal and seasonal) and spatial (continuum) variations in theses marsh waters. Precisely, an autonomous pCO_2 underwater sensor (C-Sense^{TM} pCO_2 sensor, PME/Turner Designs), an EXO1 multiparameter probe (YSI) and a C3-submersible fluorimeter (Turner Designs) were used to measure water pCO_2, chemicophysical parameters and Chlorophyll *a* (Chl *a*) concentrations respectively (Figure 7). The C-Sense sensor functions through the diffusion of the gas across a hydrophobic membrane into an isolated headspace. While any gas may enter into the headspace, the wavelength of the infrared sensor is specific to CO_2 absorption. The amount of absorption of that wavelength is proportional to the concentration of CO_2 gas in the headspace (Turner Designs). The measurement range of the C-Sense is 0-2000 ppmv with an absolute accuracy of 60 ppmv (3% of the full scale) (Turner Designs). The EXO1 probe allowed the measurement of pH (NBS scale), temperature (T in °C), salinity (S), oxygen concentration (O_2 in $mg.L^{-1}$), oxygen saturation percentage (O_2-sat in %) and turbidity (TU in in NTU). The maximum permissible error (MPE) of the different EXO1 sensors are 0.2 and 0.5 unit for the pH and the S respectively, 0.25 °C for the T, 5 NTU for the TU and 0.8 $mg.L^{-1}$ for O_2 (YSI). Furthermore, the C3-submersible fluorimeter was used to measure sub-surface water Chl *a* concentrations every ten minutes as a proxy to study phytoplankton dynamics over time. This sensor was used only for summer 2019 and winter 2020 (Table S1).

An atmospheric Eddy Covariance (EC) station (Campbell) was installed in June 2019 by Ifremer within the maritime area's NNR on salt marshes of the Bossys perdus (station *e* in Figure 6 and 7-D) to measure *in situ* CO_2 fluxes at the marsh-atmosphere and water-atmosphere exchange interfaces and, *in fine*, to study their metabolism at the ecosystem scale from a regional carbon budget point of view. The meteorological data of the EC station were used for water pCO_2 correction and water-air CO_2 flux estimation (see 2.3.) only for summer 2019 and winter 2020 (Table S1). For all other deployments (Table S1), meteorological data come from a Meteo France station (*infoclimat.fr*) located nearby in La Rochelle city (27 km).

Figure 7: (A) Home-made floating bathy equipped with C-Sense, EXO1 and C3 Fluorimeter probes; **(B)** C3-submersible Fluorimeter (Turner Designs); **(C)** C-Sense sensor and his logger (PME/Turner Designs); **(D)** Atmospheric EC station (Campbell) on salt marshes of Bossys perdus (NNR) (station *e*, Figure 6); **(E)** EXO1 multiparameter probe (YSI); **(F)** Aquatic miniPAR (PME).

2.3. Water pCO_2 correction and water-atmosphere CO_2 flux estimation

2.3.1. TDGP correction on measured pCO_2

pCO_2 values measured by the C-Sense probe are influenced by the total dissolved gas pressure (T.D.G.P.). It is the total pressure exhibited by all gasses within the water column. When this pressure greatly exceeds the pressure at which the C-Sense was calibrated, the output of the C-Sense should be corrected. Then a correction was applied according to equation (1) (Turner Designs):

(1) $pCO2 = pCO2(meas.) \times \frac{1009}{TDGP}$

(2) $TDGP = P(atm.) + P(sat.)$

(3) $P(sat.) = \exp\left(13.7 - \frac{5120}{T}\right) \times 1013.25$

With $pCO2$ the corrected pCO_2 (in ppmv); $pCO2(meas.)$ the measured pCO_2 by the C-Sense probe (in ppmv); 1009 hPa the atmospheric pressure during the day of the sensor calibration; *TDGP* the total dissolved gas pressure in water (in hPa); $P(atm.)$ the atmospheric pressure during the day of the measurement (in hPa); $P(sat.)$ the theoretical saturation steam pressure (in hPa, from Dupré-Rankine equation); T the water temperature (in K).

2.3.2. Temperature versus non-temperature effects on diurnal pCO_2 variations

To distinguish temperature and non-temperature effects on diurnal pCO_2 variations, $TpCO_2$ and $NpCO_2$ were calculated respectively according to (4) and (5) (Takahashi et *al.*, 2002). $TpCO_2$ is associated to the temperature physical effects on water pCO_2 (physical pump, see 1.3.1.). On the contrary, $NpCO_2$ corresponds to pCO_2 variations related to non-temperature effects, i.e. biological processes, tidal advection and benthos-pelagos exchanges which may be important in shallow coastal systems such as marshes (Cotovicz Jr. et *al.*, 2015).

(4) $TpCO2 = pCO2(mean) \times \exp[0.0423 \times (T - T(mean)]$

(5) $NpCO2 = pCO2 \times \exp[0.0423 \times (T(mean) - T)]$

With $TpCO2$, pCO_2 variations related to the physical effects of temperature (in ppmv); $NpCO2$, pCO_2 variations related to the non-temperature effects (in ppmv); $pCO2(mean)$ and $T(mean)$ the mean pCO_2 and temperature respectively over the 24-hour cycle.

2.3.3. CO_2 flux calculations

CO_2 flux at the water-air interface were estimated according to Polsenaere et *al.* (2013):

(6) $FCO2 = CO2solulility \times k \times [pCO2(water) - pCO2(atm.)]$

With $FCO2$ the CO_2 fluxes at the water-atmosphere interface (in $mmol.m^2.h^{-1}$); $CO2solulility$ the CO_2 solubility coefficient in water (in $mol.Kg^{-1}.atm^{-1}$); k the CO_2 gas exchange coefficient

(in cm.h^{-1}); $pCO2(water)$ the corrected pCO_2 in water (in ppmv) and $pCO2(atm.)$ the atmospheric pCO_2 (414 ppmv in February 2020, NOAA).

The CO_2 gradient between water and atmosphere controls CO_2 fluxes according to (6). Indeed, fluxes go from the CO_2 oversaturated to the undersaturated medium (chemical pump, see 1.3.1.). The CO_2 solubility coefficient depends on water temperature and salinity and was calculated according to Weiss (1974):

(7) $$CO2\ solubility = \exp(\alpha + \beta + \gamma)$$

(8) $$\alpha = -60.2409 + \frac{93.4717 \times 100}{T}$$

(9) $$\beta = 23.3585 \times \ln\left(\frac{T}{100}\right)$$

(10) $$\gamma = S \times \left(0.023517 - 0.023656 \times \frac{T}{100 + 0.0047036 \times \left(\frac{T}{100}\right)^2}\right)$$

With T the water temperature (in K) and S the water salinity.

The k exchange coefficient (6 and 11) also controls significantly water-air CO_2 fluxes since it directly takes into account turbulence processes at the water-atmosphere exchange interface (Polsenaere et *al.*, 2013). For CO_2 flux calculations, we used the near-turbulence induced by the wind from Wanninkhof (1992) because the four study stations (Figure 6) within the Fier d'Ars are in a coastal environments close to oceanic waters conditions (open surface).

(11) $$K660 = 0.31 \times (U10)^2 \times \left(\frac{Sc}{660}\right)^{-0.5}$$

(12) $$Sc = A - B \times T + C \times (T)^2 - D \times (T)^3$$

With $K660$ the exchange coefficient according Wanninkhof (1992) (in cm.h^{-1}); $U10$ the wind speed at 10 meters (in m.s^{-1}) calculated according Amoroko et Devries (1980); Sc which describe both the water viscosity and the molecular diffusion of the subsurface layer; A = 2073.1, B = 125.62, C = 3.6276 and D = 0.043219 (Bade, 2009).

2.4. *In vivo* Chl *a* concentrations and fluorimeter data calibration

Chl *a* concentration measurements provide a simple and specific assessment of the phytoplankton biomass in the water column (Aminot and Kérouel, 2004). As we deployed a

fluorimeter sensor (Figure 7-B) that measures water fluorescence emitted from all photosynthetic organisms (Aminot et Kérouel, 2004), we thus applied a calibration procedure to deduce Chl *a* concentrations from our 10 min-water fluorescence measurements. *In situ* Chl *a* concentrations were calculated owing to significant (p-value < 0.05) linear regression lines (6 and 8 in Table S1) obtained for each deployment (summer 2019 and winter 2020) between C3-fluorimeter data and *in vivo* Chl *a* concentrations analysis from sub-surface water (eight samplings in average per each 24 hour-cycle) sampled right at the fluorescence probe. Chl *a* concentrations were analysed at laboratory following Aminot and Kérouel (2004). Water samples were filtrated (47 mm Whatman GF/C filter) and pigments were extracted in a 90% acetone solvent at the time of the filter crushing with a glass rod. After an one night stirring at 4 °C and a 20 min-centrifugation at 6000 rpm, the supernatant absorbance was measured by spectrophotometry at 665 nm giving the Chl *a* level (its absorbance peak is at 665nm).

2.5. Statistical tools and analysis

Measured data were analysed by the Microsoft Excel (https://www.microsoft.com), R-studio (https://rstudio.com) and GraphPad Prism 7 (https://www.graphpad.com) software. More precisely, Microsoft Excel was used for water pCO_2 corrections, atmospheric CO_2 flux calculations (see 2.3.) and fluorimeter data calibrations (see 2.4.). A Shapiro-Wilk test showed that all measured variables did not respect a normal distribution and therefore the application conditions of the parametric tests were not respected. Shapiro-Wilk test and all statistical comparisons such as the Wilcoxon-Mann-Whitney and Kruskal-Wallis tests were carried out by R-studio with significant level of 0.05. R-studio software was also used to perform Spearman correlation matrices (corrplot package), principal component analysis and nonmetric multidimensional scaling (PCA and NMDS respectively with FactoMineR package), the hierarchical design with water pCO_2 (lsmeans and ggplot2 packages) and permutational multivariate analysis of variance (Permanova test with vegan package). To finish, graphs were performed with GraphPad Prism.

3. Results

3.1. Spatial and temporal variations in sub-surface water pCO_2 and associated relevant biogeochemical parameters

3.1.1. Significant biogeochemical variations in studied waters of the temperate salt marsh system

In situ measurements were performed at four interconnected station waters of the Fier d'Ars intertidal Bay – Vieux Port channel – dyked salt marsh continuum (Figure 6). Annual mean oxygen concentrations at stations *a*, *b*, *c* and *d* were 8.49 ± 0.84, 7.73 ± 1.07, 7.81 ± 2.16 and 8.24 ± 2.11 mg.L^{-1} respectively. A Kruskal-Wallis non-parametric statistical test showed that the oxygen concentrations (O_2) differed significantly between stations (p-value < 0.05) exept between the stations *a* and *d* (p-value = 0.48). From winter to summer, water salinity (S) at stations *a* and *b* varied (between 27.5 and 34.7) with even more variations at stations *c* and *d* between 21.3 and 42.6 across these two seasons. The axe two of the principal component analysis (PCA) allowed to carry out a spatial discrimination of Fier d'Ars waters depending on the water turbidity (TU) and pCO_2 whose correlations with the dimension two were 0.79 and 0.87 respectively (Figure 8). In average over the year, the station *b* had the highest turbidity (TU) and pCO_2 values (11.3 ± 9.6 NTU and 462 ± 51 ppmv respectively) in comparaison to other three stations: 3.9 ± 4.6 NTU and 418 ± 57 ppmv at the station *a*, 4.9 ± 3.1 NTU and 335 ± 214 ppmv at the station *c* and 1.0 ± 0.9 NTU and 293 ± 113 ppmv at the station *d* in average respectively (Figures 8 and 9). Moreover at the spatial scale, the mean annual percentage of water CO_2 undersaturation were 14%, 11%, 72% and 83% at stations *a*, *b*, *c* and *d* respectively.

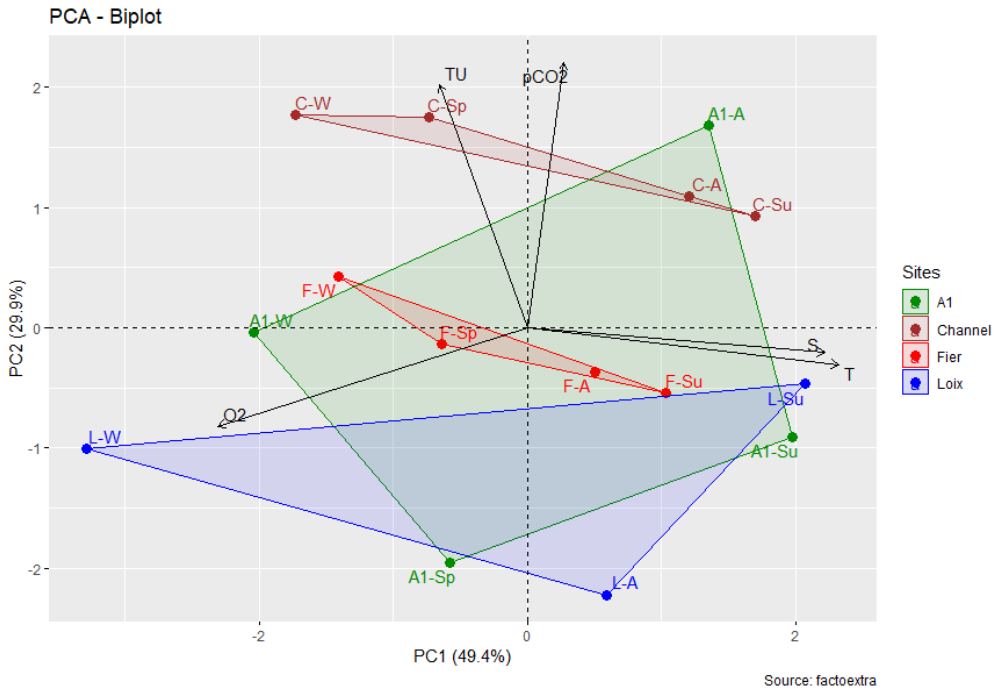

Figure 8: PCA at the spatial and seasonal scales. Axis 1 accounted for 49.4% of the information and Axis 2 accounted for 29.9%. Each point represented the "barycentre" of each measurement cycle (24 hours). Chl *a* and phaeopigments are not shown since it was not measured at stations *a* and *b* (Fier d'Ars bay and Vieux Port channel respectively).

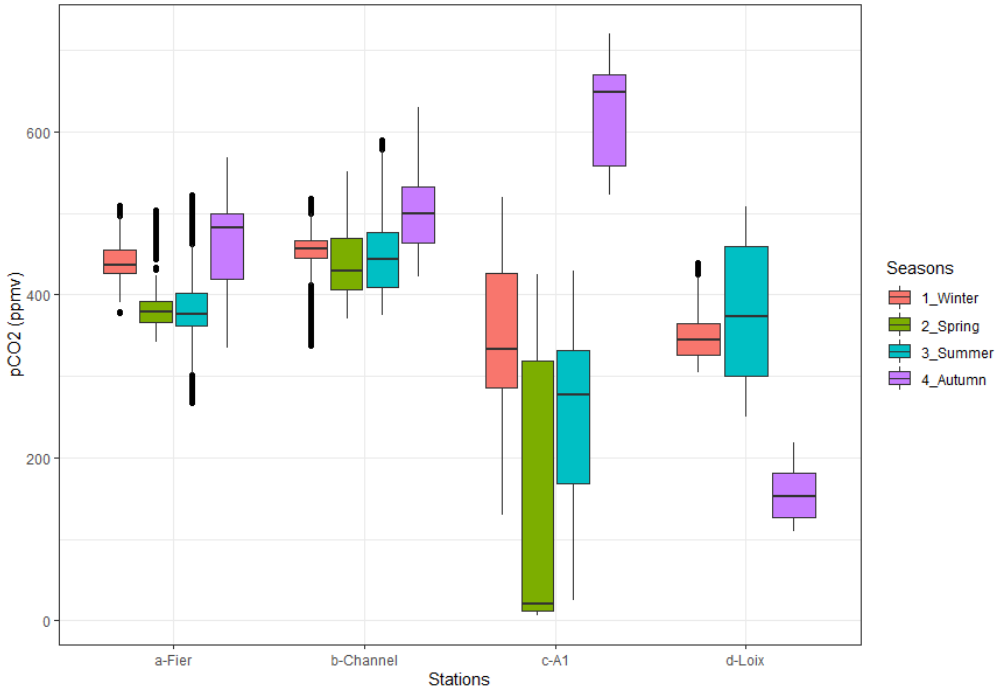

Figure 9: pCO_2 boxplot at the spatial and seasonal scales. pCO_2 (in ppmv) median, minimum and maximum values measured over each seasonal 24-hour cycle are represented at Fier d'Ars Bay, Vieux Port channel, A1 marsh and Loix marsh (stations *a*, *b*, *c* and *d* respectively). Loix marsh (station *d*) could not been studied during the 2020 spring season. Hierarchical (nested) design allowed studying (i) the spatial effect and (ii) the seasonal effect within each station on water pCO_2.

A Permutational Multivariante Analysis of Variance (Permanova) based on an Euclidean distance matrix highlighed that studied variable dispersions (temperature, salinity, turbidity, pH, oxygen concentration, oxygen saturation and pCO_2) were different for each station (p-value < 0.05). Thus, the chemicophysical and biogeochemical composition of Fier d'Ars waters significantly varied along the studied continuum. At the spatial scale, PCA in annexe 4 with Euclidean distances permitted to observe that station *b* (channel) waters were very significantly different from stations *c* and *d* waters (salt marshes) whereas station *a* waters (Fier d'Ars Bay) had similarities with other three stations (Figure 6).

3.1.2. Seasonal dynamics of the Fier d'Ars continuum waters

The axe one of the PCA (Figure 8) allowed to perform a seasonal discrimination of the different water masses along the continuum according to water T, S and O_2 values whose correlations with the dimension one were 0.91, 0.87 and -0.90 respectively. For each station, the highest T and S values were measured in summer with averages of 22.9 ± 1.6 °C and 34.2 ± 0.3 at the station *a*, 23.9 ± 1.3 °C and 34.7 ± 0.5 at the station *b*, 23.5 ± 2.5 °C and 36.8 ± 2.3 at the station *c* and 23.3 ± 1.6 °C and 35.8 ± 1.5 at the station *d*, respectively (Figure 8 and

Table S2). To the contrary, the highest O_2 values were recorded in winter with averages of 8.92 ± 0.25, 8.63 ± 0.30, 9.20 ± 0.70 and 10.06 ± 0.51 $mg.L^{-1}$ at stations *a*, *b*, *c* and *d*, respectively while summer season had the lowest O_2 values (Figure 8 and Table S2). Kruskal-Wallis tests highlighed a significant difference in water T, S and O_2 at the seasonal scale (p-values < 0.05). Over our sampling periods, Chl *a* concentrations in sub-surface waters in summer 2019 and in winter 2020 were respectively 5.21 ± 1.67 and 1.31 ± 0.27 $\mu g.L^{-1}$ at the station *c* and 1.78 ± 0.27 and 3.42 ± 0.37 $\mu g.L^{-1}$ at the station *d* respectively (Table S2). Wilcoxon-Mann-Whitney non-parametric tests highlighed that Chl *a* concentrations varied significantly between summer 2019 and winter 2020 both at stations *c* and *d* as well as photosynthetically active radiation (PAR) values (p-values < 0.05). In average, pCO_2 in winter, spring, summer and autumn were 394 ± 82, 322 ± 168, 365 ± 113 and 435 ± 181 ppmv respectively (Figure 9). Moreover, according to the hierarchical (nestes) design, pCO_2 averages differed signicantly at the seasonal scale within each station (p-value < 2.10^{-16}) except for (i) the station *a* between spring and summer (p-value = 0.93), (ii) the station *b* between winter and spring (p-value = 0.46) and (iii) the station *b* between winter and summer (p-value = 0.94) (Figure 9).

3.1.3. Biogeochemical variations in studied station waters at the diurnal/tidal scales

For all 24-hour cycles (Table S1), significant differences between day and night pCO_2 (and O_2) were highlighted by Wilcoxon-Mann-Witney tests (p-values < 0.05) (Figure 10 and Annexe 5). For instance at the diurnal scale, the respective averages of pCO_2 and O_2 at the station *b* (channel) were 481 ± 58 ppmv and 7.56 ± 1.34 $mg.L^{-1}$ the day and 447 ± 41 ppmv and 7.69 ± 0.59 $mg.L^{-1}$ the night (Figure 10) whereas at the station *c* (marsh), it were respectively of 311 ± 212 ppmv and 8.63 ± 2.23 $mg.L^{-1}$ the day and 363 ± 212 ppmv and 7.34 ± 2.22 $mg.L^{-1}$ the night, respectively (Annexe 5). To the contrary at station *c* in spring, no significant variations (p-value = 0.98) where measured with only low and constant pCO_2 values (less than 60 ppmv) most of the time and partly during the night too. Furthermore, all measurement cycles showed a decrease in pCO_2 negatively correlated to an increase in O_2 during daytime (exception at the station *c* in spring) and an opposite pattern during night-time (Figure 10 and Annexe 5). Indeed in winter, water pCO_2 at the station *c* decreased from 519 to 129 ppmv the day (from 09:00 to 17:00 the 10/02/2020) and increased from 212 to 442 ppmv the night (from 20:00 the 10/02/2020 to 05:40 the 11/02/2020). To the contrary, O_2 increased from 8.75 to 11.20 $mg.L^{-1}$ the day and decreased from 9.19 to 8.62 $mg.L^{-1}$ the night on the same periods (Figure 11).

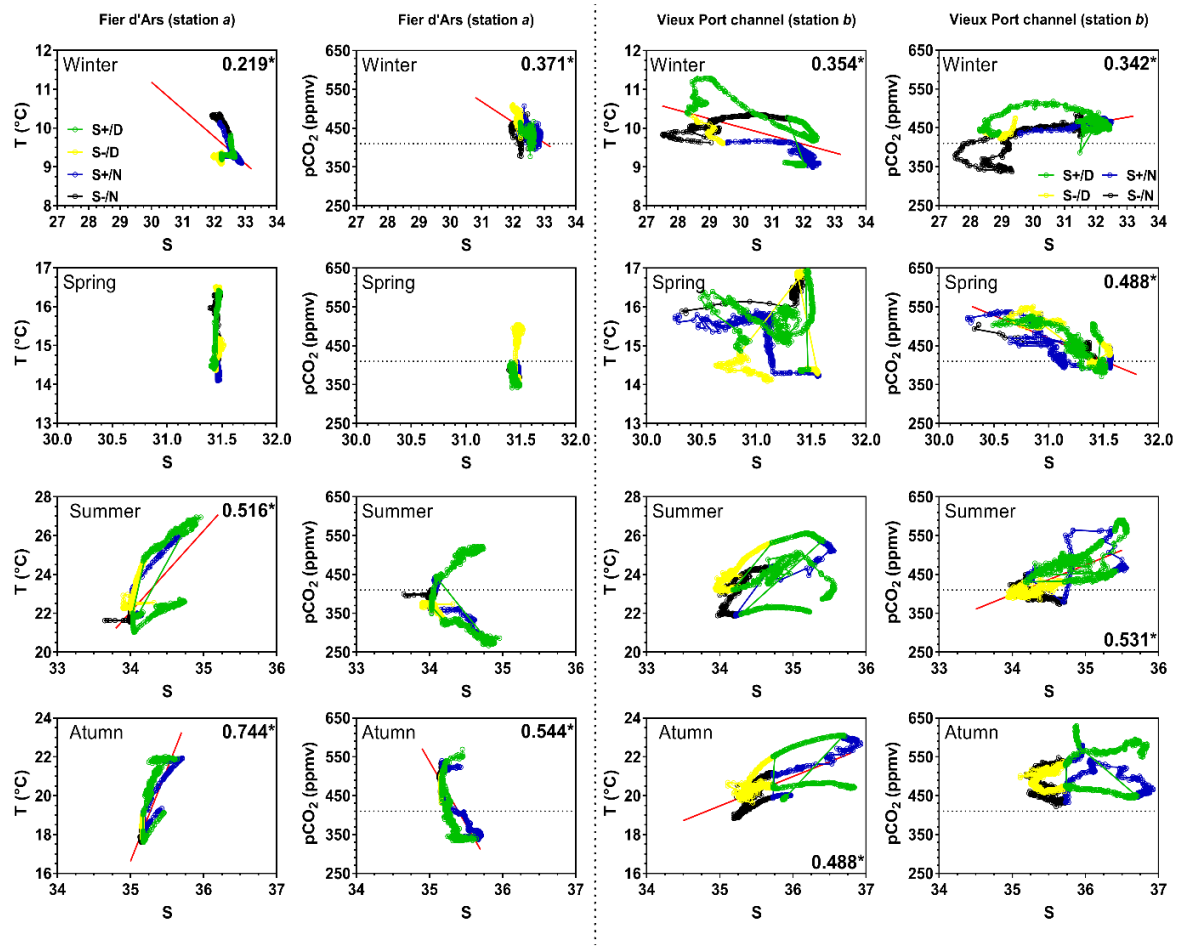

Figure 10: T/S and pCO_2/S diurnal/tidal correlation plots at stations *a* and *b*. Only significant R^2 (p-value < 0.05) are represented. Periods of high and low salinity were distinguished using the Q_{50} (median) salinity for each 24-hour cycle. S+/D: high salinity day; S-/D: low salinity day; S+/N: high salinity nigh; S-/N: low salinity nigh.

At the tidal scale, the horizontal advection of coastal waters generated an increase in water TU for all measurements cycles (Figure 11 and Annexes 6 and 7). For instance, during the first high tide of each cycle, TU varied from 1 to 10 NTU, from 7.28 to 21.21 NTU, from 2.13 to 14 NTU and from 0.97 to 4.66 NTU in summer at stations *a*, *b*, *c* and *d* respectively. At station *c*, water S increased in winter with coastal water incoming (from 27.0 to 29.7 and from 27.8 to 29.3) (Figure 11) whereas it decreased during autumn, spring and summer (from 40.4 to 35.3 and from 37.1 to 33.5 in summer for instance, Annexes 6). Water TU and S at station *d* did not varied significantly both in autumn 2019 and winter 2020 (Figure 11). Finally for all 24-hour cycles (Table S1), significant variations in water pCO_2 (p-values < 0.05) were recorded at the tidal scale i.e. between pCO_2 values lowest and highest salinity Q_{50} (median). In particular during the day, station *c* showed higher pCO_2 values at low S (S-) than at strong S (S+) values and vice versa (i) in spring (277 ± 118 and 14 ± 4 ppmv at S- and S+ respectively) and (ii) in

summer (351 ± 25 and 91 ± 53 ppmv at S- and S+ respectively) (Annexe 5). To the contrary, the reserve trend was observed at station *b* in summer (407 ± 9 and 493 ± 43 ppmv at S- and S+ respectively) (Figure 10).

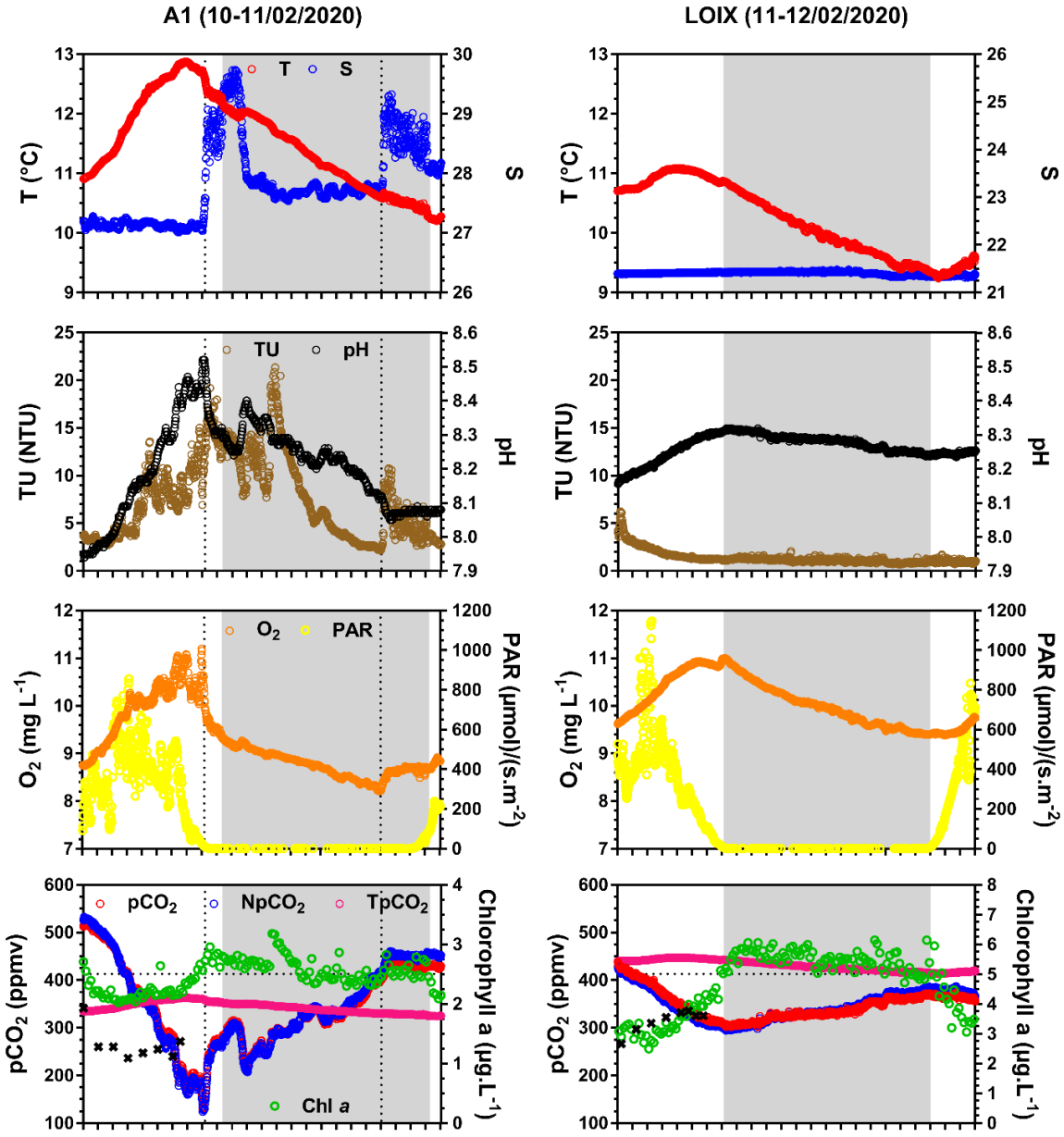

Figure 11: Temporal variations in water temperature (T, °C), salinity (S), turbidity (TU, NTU), pH, oxygen concentration (O_2, mg.L^{-1}), photosynthetically active radiation (PAR, µmol.s^{-1}.m^{-2}), pCO_2, $NpCO_2$, $TpCO_2$ (ppmv) and chlorophyll *a* concentrations (Chl *a*, µg.L^{-1}) during 24-hour cycles at stations *c* and *d* respectively (A1 and Loix salt marshes) in winter 2020. The water S and Chl *a* scales are not the same between the two stations. The black crosses represent Chl *a* measured in the laboratory from water samples (*in vivo*). Grey areas correspond to the night period. The vertical dotted lines correspond to coastal water incoming into the marshes at each high tide. The horizontal dotted lines correspond to CO_2 atmospheric concentration measured at the EC station (station *e*, Figure 6).

For all cycles, the very low ($\Delta TpCO_2/\Delta NpCO_2$) ratio (< 1) and strong positive correlations between pCO_2 and $NpCO_2$ showed a strong control of non-temperature effects on water pCO_2. Similarly, correlation matrix showed that pCO_2 were strongly and negatively correlated with O_2 and annual mean Spearman correlations between pCO_2 and O_2 were -0.87 ± 0.15, -0.78 ± 0.05, -0.49 ± 0.24 and -0.75 ± 0.07 at stations *a*, *b*, *c* and *d* respectively. At last, at station *c* in summer, correlations between pCO_2/O_2 and pCO_2/PAR were -0.15 and -0.69 respectively. Significant linear regressions were also computed between pCO_2 and S, i.e. positive both in winter and summer at station *b* (R^2 = 0.34 and R^2 = 0.53 respectively) and negative in spring (R^2 = 0.49, Figure 10). A negative pCO_2 versus S regression was also computed at station *c* both in spring and summer (R^2 = 0.83 and R^2 = 0.87 respectively) along with a positive water pCO_2 versus water height correlation (R^2 = 0.72) observed at station c in summer (Annexe 6).

3.2. Variations in estimated CO_2 exchanges at the water-air interface over the studied temperate salt marsh continuum

3.2.1. Wind speeds and exchange coefficients

Over our measurement periods, average wind speeds were 18 ± 8, 15 ± 6, 23 ± 6 and 24 ± 14 $km.h^{-1}$ at stations *a*, *b*, *c* and *d* respectively (Table S3). In winter of the year 2018, from one day to another, wind speeds dit not varied significantly between stations *a* and *b* (p-value = 0.05) whereas it significantly decreased between stations *c* and *d* in 2020 (from 27 ± 5 to 15 ± 5 $km.h^{-1}$, p-value < 0.05) (Table S3). Moreover, there was not significant variation between stations in summer (15 ± 4, 16 ± 6, 13 ± 4 and 15 ± 6 $km.h^{-1}$ at stations *a*, *b*, *c* and *d* respectively). Annual means of exchange coefficients (k660) estimated according to Wanninkhof (1992) were 8.49 ± 6.53, 6.34 ± 5.40, 13.54 ± 11.31 and 16.83 ± 17.22 $cm.h^{-1}$ at stations *a*, *b*, *c* and *d* respectively. Interestingly over all 24-hour cycles, the highest and lowest wind speeds and K660 values were observed in autumn and summer respectively (Table S3).

3.2.2. Water-air CO_2 flux variations and associated salt marsh metabolism

Water-atmosphere CO_2 flux (FCO_2) annual means along the coastal waters-marsh waters continuum were -0.03 ± 0.17, +0.16 ± 0.24, +0.04 ± 0.36 and -0.28 ± 0.38 $mmol.m^2.h^{-1}$ at stations *a*, *b*, *c* and *d* respectively, with the highest and lowest flux values estimated in autumn and summer respectively (Table S3). Annually, stations *a* and *d* behaved as a CO_2 sink (FCO_2

< 0) whereas stations *b* and *c* emitted CO_2 to atmosphere (CO_2 source function, $FCO_2 > 0$). A significant difference between CO_2 flux annual means was highlighed between stations *a*-*b* (intertidale zone, Figure 6) and stations *c*-*d* (dyked salt marshes) (p-value < 0.05). Station typology along the studied continuum thus significantly influenced the inorganic carbon behaviour and associated metabolisms at studied stations**.** In addition, estimated FCO_2 between stations *a* and *b* varied significantly at each season except in winter 2019 (p-value = 0.29). Stations *c* and *d* showed the same trend with significant variations in FCO_2 except in winter 2020 (p-value = 0.27) (Figure 12).

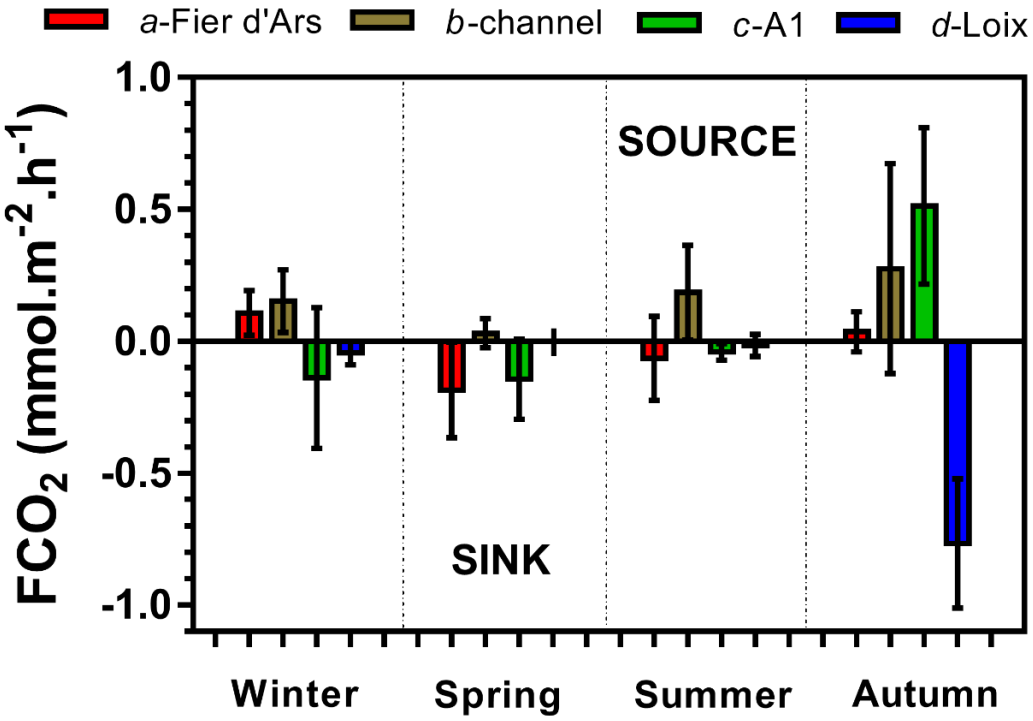

Figure 12: Seasonal and spatial variations (from 2018 to 2020) in estimated CO_2 fluxes (FCO_2, in $mmol.m^{-2}.h^{-1}$) during a 24-hour cycle at the water-atmosphere interface at stations *a*, *b*, *c* and *d*. If $FCO_2 > 0$, then the station emits CO_2 to atmosphere and if $FCO_2 < 0$, then the station absorbs CO_2 in column water. The FCO_2 were estimated according to Takahashi et *al.* (2013). Means and associated ranges over 24-hour are represented.

Station *a* had in average positive FCO_2 values both in winter and autumn (+0.10 ± 0.08 and +0.03 ± 0.07 $mmol.m^2.h^{-1}$ respectively) but negative mean values in spring and in summer (-0.18 ± 0.18 and -0.06 ± 0.16 $mmol.m^2.h^{-1}$ respectively) (Figure 12 and Table S3). At station *a*, a kruskal-Wallis test showed that FCO_2 varied significantly at the seasonal scale except (i) between spring and summer 2018 (p-value = 0.34) and (ii) between summer and autumn 2018 (p-value = 0.46). Positive FCO_2 values were measured in average at station *b* over our four

2018 measurement cycles with the highest FCO_2 values observed in autumn (+0.27 ± 0.40 $mmol.m^2.h^{-1}$) (Figure 12 and Table S3). This CO_2 source function at this station was particularly associated to a strong water-air pCO_2 gradient. At station *b*, a kruskal-Wallis test showed that FCO_2 differed significantly at the seasonal scale except between summer (-0.03/0.61 $mmol.m^2.h^{-1}$ (min/max)) and autumn (0.01/1.43 $mmol.m^2.h^{-1}$) in 2018 (p-value > 0.99). Station *c* behaved as a CO_2 sink in spring, summer 2019 and in winter 2020 whereas it emitted CO_2 to atmosphere in autumn 2019 (0.51 ± 0.30 $mmol.m^2.h^{-1}$) (Figure 12 and Table S3). FCO_2 values at A1 marsh varied between 0.15 and 1.17 $mmol.m^2.h^{-1}$ in autumn 2019 and between -0.71 and 0.33 $mmol.m^2.h^{-1}$ in winter 2020 at the diurnal scale. Finally, station *d* behaved as CO_2 sink both in winter, summer and autumn 2019 with the largest negative flux in autumn where fluxes varied between -1.35 and -0.41 $mmol.m^2.h^{-1}$ (Figure 12 and Table S3). Salt marsh FCO_2 therefore varied significantly at the seasonal and dirunal scales (p-values < 0.05). Actually, FCO_2 of station *d* were -0.87 ± 0.17 and -0.67 ± 0.15 $mmol.m^2.h^{-1}$ the day and the night respectively in autumn 2019.

4. Discussion

4.1. Differential influence of station typology on water CO_2 dynamics over the studied marsh-channel-bay continuum

Within the studied temperate salt marsh system on the Ré Island, the Vieux Port channel located between the dyked salt marshes and the Fier d'Ars Bay (Figure 6) had repeated and significant CO_2 oversaturation periods in 2018 where high water TU limited the phytoplankton activity in the water column. The strong influence of the microbial loop-type trophic network in the Fier d'Ars coastal waters (COP/Chl *a* > 200) highlighted by Tortajada (2011) promoted this CO_2 oversaturation in the Vieux Port channel by organic matter mineralisation from mudflats. Moreover, the Roc channel waters used for aquafarming activities on Les Portes en Ré city communicate with Vieux Port channel and could have enriched station *b* waters in nutrients (Tortajada, 2011) promoting also microbial respiration processes. Station *a* in the Fier d'Ars Bay had the same typology and configuration as station *b*, i.e. channel-type stations but this larger channel station, located at the entrance of the Bay is more influenced by buffered marine waters from the Breton Sound. Then, station *a* waters were less oversaturated in CO_2 than station *b* waters in 2018. Actually, CO_2 oversaturation percentages varied between 96% (winter) and 15% (spring) at station *a* whereas it varied between 70% (spring) and 100% (autumn) at station *b*. This water pCO_2 decrease in the Fier d'Ars Bay at the seasonal scale

related to favourable environmental conditions of phytoplankton in the water column where Chl *a* concentrations varied from 0.2 to 3.5 µg.L^{-1} in spring/summer (Bel Hassen, 2000). In an intertidal zone of Charentais Sounds, Savelli et *al.* (2019) showed that developed microphytobenthos biomass in mudflats was strongly resuspended in the water column by tidal effects contributing to CO_2 reduction by photosynthesis. By comparison, Coignot et *al.* (2020) showed that the Curé Canal (channel) and Aiguillon Bay (estuary) whose waters supplied Breton Sound had pCO_2 means respectively of 1873 ± 1092 ppmv (426/416 (min/max)) and 685 ± 442 ppmv (215/1929) in 2018.

Contrary to the studied stations *a* and *b*, significant CO_2 undersaturation periods were recorded in general at dyked coastal marshes (78% in average over a year at stations *c* and *d*). Photosynthesis of aquatic vegetation (*Ruppia maritima*) and phytoplankton communities under lower tidal hydrodynamic conditions, contributed to marsh primary production and CO_2 assimilation (Tobias and Neubauer, 2019). Indeed, temperate coastal wetlands such as salt marshes are autotrophic systems (NEP > 0) with low pCO_2 values in contrast to estuaries/bays (Artigas et *al.*, 2015; Najjar et *al.*, 2018). In a mangrove type ecosystem (wetland) in Nagada Creek, Borges (2003) measured pCO_2 values between 540 and 1680 ppmv in summer 2000.

4.2. Contrasted carbon process dynamics according to management practices

The pCO_2 significant variations measured between the two dyked salt marshes (stations *c* and *d*) both in summer and autumn 2019 were mainly related to primary producer activity and their fate in the water column. The A1 marsh protected inside the NNR and under water lock management was characterized by an important macroalgae development from spring to late summer, the last two years of 2019 and 2020. Thus, it strongly promoted CO_2 consumption through photosynthesis, particularly in spring and summer (134 ± 165 and 242 ± 116 ppmv respectively) along with long periods of undersaturation over tidal/diurnal cycles (100% of CO_2 undersaturation both over the spring and summer cycles). Water pCO_2 reached in turn very low values rarely observed over other wetland types. In fresh- and brackish-water marshes in the Charente Maritime department during summer of the year 2018, Ternon et *al.* (2018) measured in average 773 ± 512 and 1050 ± 566 ppmv at stations T5 and C2 respectively. The dyked-marsh station *d* differed from station *c* as salt is produced in there and it is directly connected to the Bay without channel. Except during autumn, mean water pCO_2 at station *d* were always above pCO_2 values measured at station *c* (Table S2). A strong mesoplankton development was

recorded at station *d* in summer 2019 (~59 500 individual.m^{-3}; Dupuy et *al.*, in prep.) producing a phytoplanktonic cell degradation confirmed by (i) high phaeopigments / Chl *a* ratio (0.21 in average) and (ii) a strong POC percentage (52.62%, Dupuy et *al.*, in prep.). It could then explain the larger pCO2 values difference observed between both stations *c* and *d* at this season. With regards to autumn season in 2019 at station *d*, *ruppia* seagrass and phytoplankton photosynthetic activity maintained very low pCO_2 values whereas macroalgae degradation by microbial mineralisation at A1 marsh produced high pCO_2 values and larger water oversaturation periods (100% of measurement cycle in autumn 2019). The higher ammonium concentrations in A1 marsh waters (59.70 µmol.L^{-1}, Dupuy et *al.*, in prep.) at this period confirmed the organic matter degradation.

4.3. Strong biological influence on diurnal water CO_2 dynamics

Over all measurement cycles performed at the Fier d'Ars coastal wetland continuum, both strong $NpCO_2$ variations and significant negative correlations between pCO_2 and O_2 the day and the night highlighted a strong biological control on water pCO_2 particularly in the dyked salt marshes (stations *c* and *d*). The study led by Dai et *al.*, (2009) confirmed that C biogeochemical processes in coastal environments such as the Fier d'Ars are mainly controlled by non-temperature effects as opposed to more open ocean systems where temperature effects predominate on pCO_2. Indeed the day when PAR reached high levels, the photosynthetic activity of seagrass, macroalgae and/or phytoplanktonic and microphytobenthic communities consumed CO_2 and produced O_2 in the marsh waters (Figure 11). On the contrary, the trophic network respiration during night-time produced an increase in CO_2 and an O_2 consumption. The Berg et *al.* (2019) study in a *Zostera marina* meadow measured similar significant diurnal fluctuations of water O_2 and pCO_2 related to a strong seagrass metabolisms control. Indeed at this vegetated coastal ecosystem, O_2 and pCO_2 values varied from 173 to 346 µmol.L^{-1} and from 256 to 859 ppmv respectively at the diurnal scale (Berg et *al.*, 2019) whereas it varied from 76.87 to 339.69 µmol.L^{-1} and from 25 to 430 ppmv at A1 marsh (Table S2).

4.4. Hydrodynamic interconnexion between studied stations through tidal advection

The coastal water horizontal advection characterized by an increase and a decrease in S in winter and from spring to autumn respectively, produced significant variations over all studied environmental and biogeochemical parameters at the four studied stations. Within the Fier

d'Ars wetland, the tidal variation influences on C dynamics were significant and depended on the initial biogeochemical state of water masses with regards to saturation in CO_2. For example in spring and summer of the year 2019, A1 marsh waters were largely undersaturated in CO_2 during daytime at low tide (high S), and thus incoming coastal waters from stations *a* and *b* more saturated in CO_2 produced (i) a significant increase in water pCO_2 at station *c* and (ii) an increase in TU which limited in turn phytoplankton development. These specific tidal pCO_2 variations were also highlighted during summer 2018 at station *b* in the Vieux Port channel waters where the inverse trend was observed. In fact during the daytime at high tide (low S), station *b* waters were less saturated in CO_2 than at low tide (high S), thus the flooding of coastal waters from Breton Sound induced a decrease in water pCO_2 values at the Vieux Port channel station (Figure 10). Ternon et *al.* (2018), using similar autonomous measurements over 24-hour cycles showed significant correlations of -0.95 and -0.61 between pCO_2 and the tide at Aiguillon Bay and La Rochelle harbour respectively, providing further evidence of tidal effects on the water pCO_2. Burgos et *al.* (2018) biogeochemical measurements in Cadiz Bay in Spain showed also a strong tidal control on pCO_2 with the lowest and highest values (754 and 1059 ppmv) measured at high and low tide respectively at the Sancti Petri Channel. To the contrary, no significant variations of water S and TU at Loix marsh both in autumn 2019 and winter 2020 was explained by the closure of the lock linking the marsh waters to the bay coastal waters.

4.5. Metabolism status of the studied continuum stations and associated methodological aspects

At station *b* during diurnal cycles in 2018, the several observed CO_2 oversaturation periods induced a net atmospheric CO_2 degassing from the channel waters ($+0.16 \pm 0.24$ mmol.m^2.h^{-1} in average in 2018) particularly in autumn where wind speeds and CO_2 exchange coefficients were the highest (Table S3). To the contrary, the Fier d'Ars Bay (station *a*) behaved in average as CO_2 sink both in spring and summer 2018 due to phytoplankton bloom development in coaster waters. Thus, due to their different location over the studied continuum, stations *a* and *b* at the entrance and in the back of the Bay showed contrasted metabolisms, particularly in spring-summer seasons (Figure 12). By comparison, the Curé channel located at Poitevin marshes emitted in average +7.16 mmol(CO_2).m^2.h^{-1} to the atmosphere in 2018 with strong seasonal variations (Coignot et *al.*, 2020). Similar to station *a* in terms of metabolism seasonal variations, Bozec et *al.* (2011) study over the Bay of the Brest estimated FCO_2 from +0.9 to +21.8 mmol.m^2.h^{-1} during autumn and winter and from -0.2 to -9.2 mmol.m^2.h^{-1} during spring

and summer. Moreover, strong seasonal variations in CO_2 fluxes were also observed in the Cadiz Bay with mean FCO_2 of +1.2,+ 3.6, -1.4 and +0.7 $mmol.m^2.h^{-1}$ in Jun 2006, November 2006, February 2007 and May 2007 respectively (Ribas-Ribas et *al.*, 2011). In general, the studied dyked salt marshes over the Fier d'Ars wetland behaved as an atmospheric CO_2 sink except at A1 marsh in autumn 2019. High pCO_2 values measured during 24-hour cycle at this season related to macroalgae degradation produced in turn a net CO_2 efflux to the atmosphere. To the contrary in summer of the year 2019, high water Chl *a* concentrations and a significant pCO_2/O_2 correlation computed at A1 marsh indorsed the strong control of primary producers on CO_2 absorption and an atmospheric CO_2 influx in turn. Station *d* during our measurement periods behaved as a CO_2 sink and this ecological function was promoted especially in the absence of tidal variations (closed lock) when the salt-farming activities was at a standstill (from fall to spring). Using an atmospheric eddy covariance system, Artigas et *al.* (2015) highlighted that restored salt marshes behaved as strong CO_2 sink from June to November 2011 with the highest CO_2 uptake in mid-July (-48.42 $mmol.m^2.h^{-1}$) and then as a CO_2 source from November to May 2012. In summer, no significant variations of wind speeds were observed between stations *a* and *b* in 2018 and between stations *c* and *d* in 2019 while FCO_2 varied significantly between stations. It highlighted the importance of water-air CO_2 gradient dynamic that controlled the direction of FCO_2. The marsh metabolism was thus dependent on water column CO_2 saturation (water-air gradient), the wind acting only as a driver of the flux.

For water-air CO_2 exchange estimated in this study, the exchange coefficient (k660) taking into account turbulence processes at the water-atmosphere interface (Polsenaere et *al.*, 2013) was calculated according to Wanninkhof (1992) since the Fier d'Ars wetland was located in a coastal environments close to oceanic conditions. On the contrary, in more enclosed environments such as freshwater marshes (Ternon et *al.*, 2018), the k coefficient was calculated with Raymond and Cole (2001). This methodological difference linked to the exchange coefficient parameterisation according to specific environmental conditions produced significant differences in estimated FCO_2 (Cotovicz Jr. et *al.*, 2015; Mayen, 2019). During this study, different stations were sampled along the continuum even if other type of water marsh inside the NNR or at Loix exist and should be studied too from a C dynamic point of view. For example, the atmospheric Eddy Covariance (ED) technique is deployed within NNR to measure continuously year-round *in situ* FCO_2 over the Bossys perdus salt marsh (Figure 6) and to study its metabolism under true field conditions. Over our measurement periods in summer 2019 and winter 2020 (Table S1), this innovative and non-intrusive method allows us measuring *in situ*

FCO_2 from this nearly marsh of -4.79 ± 11.79 and -4.88 ± 4.56 $mmol.m^2.h^{-1}$ respectively and thus achieving a better spatial representation of the different marshes and associated habitats.

5. Conclusion and perspectives

This present study carried out along a dyked salt marsh – channel – intertidal bay continuum in the Fier d'Ars wetland highlighted a strong biological control on water pCO_2 and associated metabolisms at diurnal and seasonal scales according to station typology and management practice too. In the schorre area, the Fier d'Ars Bay and Vieux Port channel stations (*a* and *b*) showed significant variations in water pCO_2 values, particularly in spring and summer 2018. Channel water biogeochemical (station *b*) was mainly controlled by heterotrophic organic matter mineralisation (microbial loop-type trophic network) whereas Fier d'Ars Bay waters had a significant phytoplankton bloom from spring to summer promoting CO_2 absorption by photosynthesis. In general, the studied dyked salt marshes had significant CO_2 undersaturation periods mainly related to the primary producer photosynthesis activity at the diurnal scale (macroalgae, phytoplankton and *ruppia s*eagrass). Other non-temperature effect such as coastal water tidal advection significantly influenced diurnal water CO_2 dynamics among connected stations. Annually, the studied salt marshes absorbed CO_2 from the atmosphere to the water column through an autotrophic activity except at station *c* in autumn 2019 where the microbial degradation of macroalgae caused an important CO_2 degassing. Finally according to our results, the atmospheric CO_2 sink function of a salt marsh continues toward autumn season particularly when tidal variations and macroalgae development in the water column are limited.

Further continuous diurnal/tidal measurements coupled with other techniques will allow constraining more accurately the metabolic balance and related processes of such heterogeneous and dynamic system that are salt marshes. Thus, as part of an Ifremer thesis, the EC station will be used to measure continuously *in situ* marsh sediment-air and water-air FCO_2 at the ecosystem scale. Particularly this technique will determinate metabolic processes and fluxes (the net ecosystem metabolism with gross primary production and community respiration). Furthermore, other measurements will be done simultaneously with for instance benthic chamber deployments to measure *in situ* sediment-air CO_2 fluxes but also the metabolic balance of planktonic communities. This integrative approach will provide further information on the role of terrestrial (plan marsh) and aquatic (phytoplanktonic and microphytobenthic communities, seagrass, macroalgae) metabolisms in the carbon cycle of salt marshes.

An Introduction to the Convention on Wetlands (previously The Ramsar Convention Manual). Ramsar Convention Secretariat, Gland, Switzerland.

Abril, G., Commarieu, M.-V., Sottolichio, A., Bretel, P., Guérin, F., 2009. Turbidity limits gas exchange in a large macrotidal estuary. Estuarine, Coastal and Shelf Science 83, 342–348. https://doi.org/10.1016/j.ecss.2009.03.006

AcclimaTerra, Le Treut, H. (dir). Anticiper les changements climatiques en Nouvelle-Aquitaine. Pour agir dans les territoires. Éditions Région Nouvelle-Aquitaine, 2018, 488 p.

Aminot, A., Kérouel, R., 2004. Hydrologie des écosystèmes marins: Paramètres et analyses. Ed. Ifremer, 336 p.

Artigas, F., Shin, J.Y., Hobble, C., Marti-Donati, A., Schäfer, K.V.R., Pechmann, I., 2015. Long term carbon storage potential and CO_2 sink strength of a restored salt marsh in New Jersey. Agricultural and Forest Meteorology 200, 313–321. https://doi.org/10.1016/j.agrformet.2014.09.012

Aufdenkampe, A.K., Mayorga, E., Raymond, P.A., Melack, J.M., Doney, S.C., Alin, S.R., Aalto, R.E., Yoo, K., 2011. Riverine coupling of biogeochemical cycles between land, oceans, and atmosphere. Frontiers in Ecology and the Environment 9, 53–60. https://doi.org/10.1890/100014

Bade, D.L., 2009. Gas Exchange at the Air–Water Interface, in: Encyclopedia of Inland Waters. Elsevier, pp. 70–78. https://doi.org/10.1016/B978-012370626-3.00213-1

Bauer, J.E., Cai, W.-J., Raymond, P.A., Bianchi, T.S., Hopkinson, C.S., Regnier, P.A.G., 2013. The changing carbon cycle of the coastal ocean. Nature 504, 61–70. https://doi.org/10.1038/nature12857

Bel Hassen, M., 2000. Fonctionnement des marais maritimes atlantiques: échanges d'énergie et effets des flux aquacoles diffus. PhD Thesis, Université de Bretagne Occidentale. https://archimer.ifremer.fr/doc/00450/56185/

Bel Hassen, M., 2001. Spatial and Temporal Variability in Nutrients and Suspended Material Processing in the Fier d'Ars Bay (France). Estuarine, Coastal and Shelf Science 52, 457–469. https://doi.org/10.1006/ecss.2000.0754

Berg, P., Delgard, M.L., Polsenaere, P., McGlathery, K.J., Doney, S.C., Berger, A.C., 2019. Dynamics of benthic metabolism, O_2 , and pCO_2 in a temperate seagrass meadow. Limnol Oceanogr 64, 2586–2604. https://doi.org/10.1002/lno.11236

Bindoff, N.L., P.A. Stott, K.M. AchutaRao, M.R. Allen, N. Gillett, D. Gutzler, K. Hansingo, G. Hegerl, Y. Hu, S. Jain, I.I. Mokhov, J. Overland, J. Perlwitz, R. Sebbari and X. Zhang, 2013: Detection and Attribution of Climate Change: from Global to Region*al*. In: Climate Change 2013: *The Physical Science Basis. Contribution of Working Group I to the Fifth Assessment Report of the Intergovernmental Panel on Climate Change* [Stocker, T.F., D. Qin, G.-K. Plattner, M. Tignor, S.K. Allen, J. Boschung, A. Nauels, Y. Xia, V. Bex and P.M. Midgley (eds.)]. Cambridge University Press, Cambridge, United Kingdom and New York, NY, USA.

Borges, A.V., 2003. Atmospheric CO_2 flux from mangrove surrounding waters. Geophys. Res. Lett. 30, 1558. https://doi.org/10.1029/2003GL017143

Bozec, Y., Merlivat, L., Baudoux, A.-C., Beaumont, L., Blain, S., Bucciarelli, E., Danguy, T., Grossteffan, E., Guillot, A., Guillou, J., Répécaud, M., Tréguer, P., 2011. Diurnal to inter-annual dynamics of pCO_2 recorded by a CARIOCA sensor in a temperate coastal ecosystem (2003–2009). Marine Chemistry 126, 13–26. https://doi.org/10.1016/j.marchem.2011.03.003

Burgos, M., Ortega, T., Forja, J., 2018. Carbon Dioxide and Methane Dynamics in Three Coastal Systems of Cadiz Bay (SW Spain). Estuaries and Coasts 41, 1069–1088. https://doi.org/10.1007/s12237-017-0330-2

Cai, W.-J., 2011. Estuarine and Coastal Ocean Carbon Paradox: CO_2 Sinks or Sites of Terrestrial Carbon Incineration? Annu. Rev. Mar. Sci. 3, 123–145. https://doi.org/10.1146/annurev-marine-120709-142723

Cai, W.-J., Pomeroy, L.R., Moran, M.A., Wang, Y., 1999. Oxygen and carbon dioxide mass balance for the estuarine-intertidal marsh complex of five rivers in the southeastern U.S. Limnol. Oceanogr. 44, 639–649. https://doi.org/10.4319/lo.1999.44.3.0639

Champion, E., Gernigon, J., Lemesle, J.C., Terrisse, J., Maisonhaute, S., 2012. 3ème Plan de gestion 2013-2017 de la réserve naturelle nationale de Lilleau des Niges.

Chapin, F.S., Woodwell, G.M., Randerson, J.T., Rastetter, E.B., Lovett, G.M., Baldocchi, D.D., Clark, D.A., Harmon, M.E., Schimel, D.S., Valentini, R., Wirth, C., Aber, J.D., Cole, J.J., Goulden, M.L., Harden, J.W., Heimann, M., Howarth, R.W., Matson, P.A., McGuire, A.D., Melillo, J.M., Mooney, H.A., Neff, J.C., Houghton, R.A., Pace, M.L., Ryan, M.G., Running, S.W., Sala, O.E., Schlesinger, W.H., Schulze, E.-D., 2006. Reconciling Carbon-cycle Concepts, Terminology, and Methods. Ecosystems 9, 1041–1050. https://doi.org/10.1007/s10021-005-0105-7

Chmura, G.L., Anisfeld, S.C., Cahoon, D.R., Lynch, J.C., 2003. Global carbon sequestration in tidal, saline wetland soils. Global Biogeochem. Cycles 17, n/a-n/a. https://doi.org/10.1029/2002GB001917

Chow, A.T., Dai, J., Conner, W.H., Hitchcock, D.R., Wang, J.-J., 2013. Dissolved organic matter and nutrient dynamics of a coastal freshwater forested wetland in Winyah Bay, South Carolina. Biogeochemistry 112, 571–587. https://doi.org/10.1007/s10533-012-9750-z

Ciais, P., C. Sabine, G. Bala, L. Bopp, V. Brovkin, J. Canadell, A. Chhabra, R. DeFries, J. Galloway, M. Heimann, C. Jones, C. Le Quéré, R.B. Myneni, S. Piao and P. Thornton, 2013: Carbon and Other Biogeochemical Cycles. In: Climate Change 2013: *The Physical Science Basis. Contribution of Working Group I to the Fifth Assessment Report of the Intergovernmental Panel on Climate Change* [Stocker, T.F., D. Qin, G.-K. Plattner, M. Tignor, S.K. Allen, J. Boschung, A. Nauels, Y. Xia, V. Bex and P.M. Midgley (eds.)]. Cambridge University Press, Cambridge, United Kingdom and New York, NY, USA.

Coignot, E., Polsenaere, P., Soletchnik, P., Le Moine, O., Souchu, P., Joyeux, E., Le Roy, Y., Guéret, J.P., Froud, L., Gallais, R., Chourré, E., Chaigneau, L., 2020. Variabilité spatio-temporelle des nutriments et du carbone et flux associés le long d'un continuum terrestre-aquatique tempéré (Marais poitevin – Baie de l'Aiguillon – Pertuis Breton). Rapport final (suivi 2017-2018) - Projet Aiguillon (2016-2020). https://archimer.ifremer.fr/doc/00618/73003/

Craft, C., 2016. Creating and Restoring Wetlands: From Theory to Practice. Elsevier, Amsterdam, 348 p.

Cole, J.J., Prairie, Y.T., Caraco, N.F., McDowell, W.H., Tranvik, L.J., Striegl, R.G., Duarte, C.M., Kortelainen, P., Downing, J.A., Middelburg, J.J., Melack, J., 2007. Plumbing the Global Carbon Cycle: Integrating Inland Waters into the Terrestrial Carbon Budget. Ecosystems 10, 172–185. https://doi.org/10.1007/s10021-006-9013-8

Cotovicz Jr., L.C., Knoppers, B.A., Brandini, N., Costa Santos, S.J., Abril, G., 2015. A strong CO_2 sink enhanced by eutrophication in a tropical coastal embayment (Guanabara Bay, Rio de Janeiro, Brazil). Biogeosciences 12, 6125–6146. https://doi.org/10.5194/bg-12-6125-2015

Crosswell, J.R., Anderson, I.C., Stanhope, J.W., Van Dam, B., Brush, M.J., Ensign, S., Piehler, M.F., McKee, B., Bost, M., Paerl, H.W., 2017. Carbon budget of a shallow, lagoonal estuary: Transformations and source-sink dynamics along the river-estuary-ocean continuum: Carbon budget of a shallow estuary. Limnol. Oceanogr. 62, S29–S45. https://doi.org/10.1002/lno.10631

Denman, K.L., G. Brasseur, A. Chidthaisong, P. Ciais, P.M. Cox, R.E. Dickinson, D. Hauglustaine, C. Heinze, E. Holland, D. Jacob, U. Lohmann, S Ramachandran, P.L. da Silva Dias, S.C. Wofsy and X. Zhang, 2007: Couplings Between Changes in the Climate System and Biogeochemistry. In: Climate Change 2007: *The Physical Science Basis. Contribution of Working Group I to the Fourth Assessment Report of the Intergovernmental Panel on Climate Change* [Solomon, S., D. Qin, M. Manning, Z. Chen, M. Marquis, K.B. Averyt, M.Tignor and H.L. Miller (eds.)]. Cambridge University Press, Cambridge, United Kingdom and New York, NY, USA.

Dai, M., Lu, Z., Zhai, W., Chen, B., Cao, Z., Zhou, K., Cai, W.-J., Chenc, C.-T.A., 2009. Diurnal variations of surface seawater pCO2 in contrasting coastal environments. Limnol. Oceanogr. 54, 735–745. https://doi.org/10.4319/lo.2009.54.3.0735

Denman, K.L., Brasseur, G., Chidthaisong, A., Ciais, P., Cox, P.M., Dickinson, R.E., Hauglustaine, D., Heinze, C., Holland, E., Jacob, D., Lohmann, U., Ramachandran, S., Archer, D., Arora, V., Austin, J., Baker, D., Berry, J.A., Betts, R., Bonan, G., Bousquet, P., Canadell, J., Christian, J., Clark, D.A., Dameris, M., Dentener, F., Easterling, D., Eyring, V., Feichter, J., Friedlingstein, P., Fung, I., Fuzzi, S., Gong, S., Gruber, N., Guenther, A., Gurney, K., Henderson-Sellers, A., House, J., Jones, A., Jones, C., Kärcher, B., Kawamiya, M., Lassey, K., Leck, C., Lee-Taylor, J., Malhi, Y., Masarie, K., McFiggans, G., Menon, S., Miller, J.B., Peylin, P., Pitman, A., Quaas, J., Raupach, M., Rayner, P., Rehder, G., Riebesell, U., Rödenbeck, C., Rotstayn, L., Roulet, N., Sabine, C., Schultz, M.G., Schulz, M., Schwartz, S.E., Steffen, W., Stevenson, D., Tian, Y., Trenberth, K.E., Noije, T.V., Wild, O., Zhang, T., Zhou, L., Boonpragob, K., Heimann, M., Molina, M., n.d. Couplings Between Changes in the Climate System and Biogeochemistry 90.

Environmental Protection Agency (EPA): https://www.epa.gov/wetlands/classification-and-types-wetlands#marshes [in line 01/05/2020]

Fagherazzi, S., Wiberg, P.L., Temmerman, S., Struyf, E., Zhao, Y., Raymond, P.A., 2013. Fluxes of water, sediments, and biogeochemical compounds in salt marshes. Ecol Process 2, 3. https://doi.org/10.1186/2192-1709-2-3

Frankignoulle, M., Abril, G., Borges, A., Bourge, I., Canon, C., Delille, B., Libert, E., Théate, J.-M., 1998. Carbon Dioxide Emission from European Estuaries. Science, New Series 282, 434–436.

Friedlingstein, P., Jones, M.W., O'Sullivan, M., Andrew, R.M., Hauck, J., Peters, G.P., Peters, W., Pongratz, J., Sitch, S., Le Quéré, C., Bakker, D.C.E., Canadell, J.G., Ciais, P., Jackson, R.B., Anthoni, P., Barbero, L., Bastos, A., Bastrikov, V., Becker, M., Bopp, L., Buitenhuis, E., Chandra, N., Chevallier, F., Chini, L.P., Currie, K.I., Feely, R.A., Gehlen, M., Gilfillan, D., Gkritzalis, T., Goll, D.S., Gruber, N., Gutekunst, S., Harris, I., Haverd, V., Houghton, R.A., Hurtt, G., Ilyina, T., Jain, A.K., Joetzjer, E.,

Kaplan, J.O., Kato, E., Klein Goldewijk, K., Korsbakken, J.I., Landschützer, P., Lauvset, S.K., Lefèvre, N., Lenton, A., Lienert, S., Lombardozzi, D., Marland, G., McGuire, P.C., Melton, J.R., Metzl, N., Munro, D.R., Nabel, J.E.M.S., Nakaoka, S.-I., Neill, C., Omar, A.M., Ono, T., Peregon, A., Pierrot, D., Poulter, B., Rehder, G., Resplandy, L., Robertson, E., Rödenbeck, C., Séférian, R., Schwinger, J., Smith, N., Tans, P.P., Tian, H., Tilbrook, B., Tubiello, F.N., van der Werf, G.R., Wiltshire, A.J., Zaehle, S., 2019. Global Carbon Budget 2019. Earth Syst. Sci. Data 11, 1783–1838. https://doi.org/10.5194/essd-11-1783-2019

Furukawa, Y., Inubushi, K., Ali, M., Itang, A.M., Tsuruta, H., 2005. Effect of changing groundwater levels caused by land-use changes on greenhouse gas fluxes from tropical peat lands. Nutr Cycl Agroecosyst 71, 81–91. https://doi.org/10.1007/s10705-004-5286-5

Gattuso, J.-P., Frankignoulle, M., Wollast, R., 1998. CARBON AND CARBONATE METABOLISM IN COASTAL AQUATIC ECOSYSTEMS. Annu. Rev. Ecol. Syst. 29, 405–434. https://doi.org/10.1146/annurev.ecolsys.29.1.405

Guérin, F., Abril, G., Serça, D., Delon, C., Richard, S., Delmas, R., Tremblay, A., Varfalvy, L., 2007. Gas transfer velocities of CO2 and CH4 in a tropical reservoir and its river downstream. Journal of Marine Systems 66, 161–172. https://doi.org/10.1016/j.jmarsys.2006.03.019

He, B., Dai, M., Zhai, W., Wang, L., Wang, K., Chen, J., Lin, J., Han, A., Xu, Y., 2010. Distribution, degradation and dynamics of dissolved organic carbon and its major compound classes in the Pearl River estuary, China. Marine Chemistry 119, 52–64. https://doi.org/10.1016/j.marchem.2009.12.006

Honeywill, C., Paterson, D., Hagerthey, S., 2002. Determination of microphytobenthic biomass using pulse-amplitude modulated minimum fluorescence. European Journal of Phycology 37, 485–492. https://doi.org/10.1017/S0967026202003888

Howarth, R., Chan, F., Conley, D.J., Garnier, J., Doney, S.C., Marino, R., Billen, G., 2011. Coupled biogeochemical cycles: eutrophication and hypoxia in temperate estuaries and coastal marine ecosystems. Frontiers in Ecology and the Environment 9, 18–26. https://doi.org/10.1890/100008

IPCC, 2000 – Robert T. Watson, Ian R. Noble, Bert Bolin, N. H. Ravindranath, David J. Verardo and David J. Dokken (Eds.) Cambridge University Press, UK. pp 375 Available from Cambridge University Press, The Edinburgh Building Shaftesbury Road, Cambridge CB2 2RU ENGLAND

Juppin, J., 2018. Evolution morpho-sédimentaire des marais des Pertuis Charentais à l'échelle pluri-décennale. Master's degree internship report, LIENSs.

Macreadie, P.I., Serrano, O., Maher, D.T., Duarte, C.M., Beardall, J., 2017. Addressing calcium carbonate cycling in blue carbon accounting: Addressing $CaCO_3$ cycling in blue CO_2 accounting. Limnol. Oceanogr. 2, 195–201. https://doi.org/10.1002/lol2.10052

Mayen, J., 2019. Variabilité temporelle des pressions partielles de CO_2 dans l'eau et flux eau-atmosphère associés au niveau des marais du Fier d'Ars (île de Ré). Master's degree internship report, Ifremer. https://archimer.ifremer.fr/doc/00505/61678/

Mcleod, E., Chmura, G.L., Bouillon, S., Salm, R., Björk, M., Duarte, C.M., Lovelock, C.E., Schlesinger, W.H., Silliman, B.R., 2011. A blueprint for blue carbon: toward an improved understanding of the role of vegetated coastal habitats in sequestering CO_2. Frontiers in Ecology and the Environment 9, 552–560. https://doi.org/10.1890/110004

Mendelssohn, I.A., Morris, J.T., 2002. Eco-Physiological Controls on the Productivity of Spartina Alterniflora Loisel, in: Weinstein, M.P., Kreeger, D.A. (Eds.), Concepts and Controversies in Tidal Marsh Ecology. Kluwer Academic Publishers, Dordrecht, pp. 59–80. https://doi.org/10.1007/0-306-47534-0_5

Najjar, R.G., Herrmann, M., Alexander, R., Boyer, E.W., Burdige, D.J., Butman, D., Cai, W.-J., Canuel, E.A., Chen, R.F., Friedrichs, M.A.M., Feagin, R.A., Griffith, P.C., Hinson, A.L., Holmquist, J.R., Hu, X., Kemp, W.M., Kroeger, K.D., Mannino, A., McCallister, S.L., McGillis, W.R., Mulholland, M.R., Pilskaln, C.H., Salisbury, J., Signorini, S.R., St-Laurent, P., Tian, H., Tzortziou, M., Vlahos, P., Wang, Z.A., Zimmerman, R.C., 2018. Carbon Budget of Tidal Wetlands, Estuaries, and Shelf Waters of Eastern North America. Global Biogeochem. Cycles 32, 389–416. https://doi.org/10.1002/2017GB005790

National Oceanic and Atmospheric Administration (NOAA): https://oceanservice.noaa.gov/facts/saltmarsh.html [in line 01/05/2020]

Nixon, S.W., Granger, S.L., Nowicki, B.L., 1995. An assessment of the annual mass balance of carbon, nitrogen, and phosphorus in Narragansett Bay. Biogeochemistry 31. https://doi.org/10.1007/BF00000805

Newell, S.Y., Porter, D., 2000. Microbial secondary production from saltmarsh grass shoots and its known potential fates. In: Weinstein, M., Kreeger, D.A. (Eds.), Concepts and Controversies in Tidal Marsh Ecology. Kluwer Academic Publishing, Dordrecht, Netherlands, pp. 159-185.

Oustin, D., 2003. Etude et cartographie de la végétation des marais salés de l'anse d'Yffiniac. Université de Rennes I.

Paticat, F., 2007. Flux et usages de l'eau de mer dans les marais salés endigués Charentais : Cas du marais salé endigué de l'île de Ré. PhD Thesis, Université de Nantes. https://archimer.ifremer.fr/doc/00000/4518/

Polsenaere, P., 2011. Echanges de CO_2 atmosphérique dans la lagune d'Arcachon et relations avec le métabolisme intertidal (Biogéochimie et Ecosystèmes). PhD Thesis, Université de Bordeaux I.

Polsenaere, P., Deborde, J., Detandt, G., Vidal, L.O., Pérez, M.A.P., Marieu, V., Abril, G., 2013. Thermal enhancement of gas transfer velocity of CO_2 in an Amazon floodplain lake revealed by eddy covariance measurements: GAS TRANSFER VELOCITY IN AN AMAZON LAKE. Geophys. Res. Lett. 40, 1734–1740. https://doi.org/10.1002/grl.50291

Prentice, I.C., Farquhar, G.D., Fasham, M.J.R., Goulden, M.L., Heimann, M., Jaramillo, V.J., Kheshgi, H.S., Le Quéré, C., Scholes, R.J. and Wallace, D.W.R.: The Carbon Cycle and Atmospheric Carbon Dioxide. In: Climate Change 2001: The Scientific Basis. Contribution of Working Group I to the Third Assessment Report of the Intergovernmental Panel on Climate Change [Houghton, J.T., Y., Ding, D.J. Griggs, et *al.* (eds.)], Cambridge University Press, Cambridge, United Kingdom and New York, NY, USA, 185-237, 2001.

Raymond, P.A., Cole, J.J., 2001. Gas Exchange in Rivers and Estuaries: Choosing a Gas Transfer Velocity. Estuaries 24, 312. https://doi.org/10.2307/1352954

Ribas-Ribas, M., Gómez-Parra, A., Forja, J.M., 2011. Air–sea CO_2 fluxes in the north-eastern shelf of the Gulf of Cádiz (southwest Iberian Peninsula). Marine Chemistry 123, 56–66. https://doi.org/10.1016/j.marchem.2010.09.005

Savelli, R., Bertin, X., Orvain, F., Gernez, P., Dale, A., Coulombier, T., Pineau, P., Lachaussée, N., Polsenaere, P., Dupuy, C., Le Fouest, V., 2019. Impact of Chronic and Massive Resuspension Mechanisms on the Microphytobenthos Dynamics in a Temperate Intertidal Mudflat. J. Geophys. Res. Biogeosci. 124, 3752–3777. https://doi.org/10.1029/2019JG005369

Schäfer, K.V.R., Tripathee, R., Artigas, F., Morin, T.H., Bohrer, G., 2014. Carbon dioxide fluxes of an urban tidal marsh in the Hudson-Raritan estuary: Carbon dioxide fluxes of an wetland. J. Geophys. Res. Biogeosci. 119, 2065–2081. https://doi.org/10.1002/2014JG002703

Takahashi, T., Sutherland, S.C., Sweeney, C., Poisson, A., Metzl, N., Tilbrook, B., Bates, N., Wanninkhof, R., Feely, R.A., Sabine, C., Olafsson, J., Nojiri, Y., 2002. Global sea–air CO2 flux based on climatological surface ocean pCO2, and seasonal biological and temperature effects. Deep Sea Research Part II: Topical Studies in Oceanography 49, 1601–1622. https://doi.org/10.1016/S0967-0645(02)00003-6

Ternon, Q., Polsenaere, P., Le Fouest, V., Favier, J.B., Philippine, O., Chabirand, J.M., Grizon, J., Dupuy, C., 2020. Étude des pressions partielles et flux de CO_2 au sein de la Communauté d'Agglomération de La Rochelle.

Tobias, C., Neubauer, S.C., 2019. Salt Marsh Biogeochemistry—An Overview, in: Coastal Wetlands. Elsevier, pp. 539–596. https://doi.org/10.1016/B978-0-444-63893-9.00016-2

Tortajada, S., 2011. De l'étude du fonctionnement des réseaux trophiques planctoniques des marais de Charente Maritime vers la recherche d'indicateurs (Océanologie Biologie et Environnement Marin). PhD Thesis, Université de La Rochelle.

Wang, Z.A., Kroeger, K.D., Ganju, N.K., Gonneea, M.E., Chu, S.N., 2016. Intertidal salt marshes as an important source of inorganic carbon to the coastal ocean: Marsh lateral export of inorganic carbon. Limnol. Oceanogr. 61, 1916–1931. https://doi.org/10.1002/lno.10347

Wanninkhof, R., 1992. Relationship between wind speed and gas exchange over the ocean. J. Geophys. Res. 97, 7373. https://doi.org/10.1029/92JC00188

Weiss, I., 1997. Le Fier d'Ars : Approche de la variabilité des peuplements floristiques et de l'hydrologie d'une zone humide littorale anthropisée. Master's degree internship report, Ifremer. https://archimer.ifremer.fr/doc/00439/55014/

Weston, N.B., Neubauer, S.C., Velinsky, D.J., Vile, M.A., 2014. Net ecosystem carbon exchange and the greenhouse gas balance of tidal marshes along an estuarine salinity gradient. Biogeochemistry 120, 163–189. https://doi.org/10.1007/s10533-014-9989-7

Woodwell, G.M., Whittaker, R.H., 1968. Primary Production in Terrestrial Ecosystems. Am Zool 8, 19–30. https://doi.org/10.1093/icb/8.1.19

Annexes

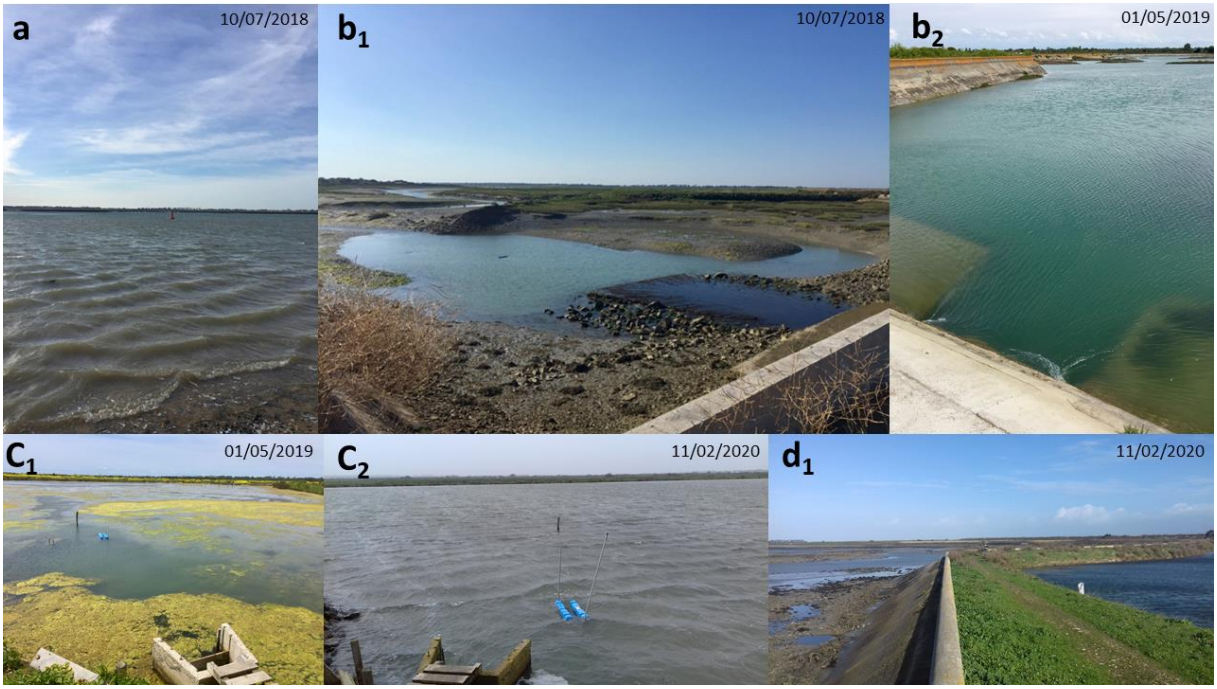

Annexe 1: Station *a*, *b*, *c* and *d* pictures (***a*:** Fier d'Ars Bay, ***b*:** Vieux Port channel downstream, ***c*:** A1 marsh, ***d*:** Loix ecomuseum marsh). **b1** and **b2** show the Vieux Port channel station at low and high tide respectively. **c1** and **c2** show A1 marsh within the NNR at two contrasted seasons with and without aquatic macroalgae respectively. **d1** allows to see the dyke separating Fier d'Ars coastal waters and Loix ecomuseum marsh.

Annexe 2: Hydraulic infrastructures of the Lilleau des Niges NNR (modified from Champion et *al.*, 2012). The blue arrow corresponds to coastal water entrance from the Vieux Port channel into the A1 marsh (*c* station, red circle).

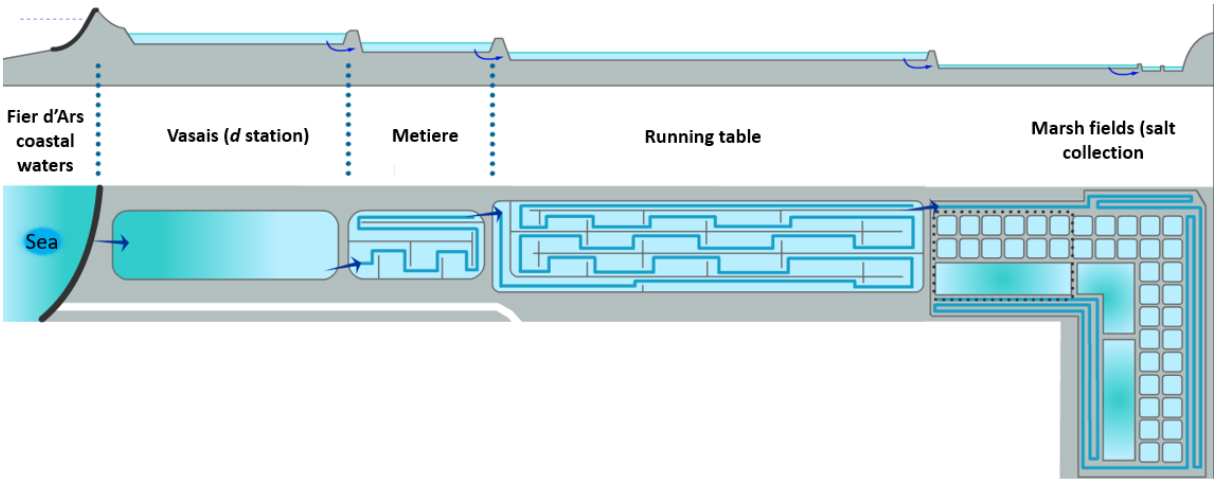

Annexe 3: Hydraulic functioning of the Loix salt marshes (station *d*) for a salt-farming activity. The coastal waters of the Fier d'Ars enter in the vasais at each high tide when the lock is open and circulate then between each marsh by gravitation (modified from Loix Ecomuseum).

Table S1: Water samplings and *in situ* measurements performed during PAMPANINO (2018) and PAMPAS (2019 and 2020) projects along Fier d'Ars bay – Vieux Port channel – salt marshes continuum (stations *a*, *b*, *c* and *d*). The deployments 5 and 6 (in bleu bellow) were carried out during the Master's degree 1 internship whereas the deployment 8 (in red bellow) was carried out during the Master's degree 2 internship. U.T. Universal time.

	Seasons and years	Stations	Dates	Cycles (U.T.)	Mean tidal coefficient
1	Winter 2018	*a*	14/03 - 15/03/2018	07:00 - 07:00	65
		b	15/03 - 16/03/2018	09:00 - 09:00	77
2	Spring 2018	*a*	25/04 - 26/04/2018	05:00 - 05:00	62
		b	26/04 - 27/04/2018	07:00 - 07:00	74
3	Summer 2018	*a*	09/07 - 10/07/2018	05:00 - 05:00	60
		b	10/07 - 11/07/2018	07:00 - 07:00	73
4	Autumn 2018	*a*	19/09 - 20/09/2018	05:00 - 05:00	36
		b	20/09 - 21/09/2018	06:30 - 06:30	45
5	**Spring 2019**	***c***	**01/05 - 02/05/2019**	**11:00 - 11:00**	**64**
6	**Summer 2019**	***c***	**16/07 - 17/07/2019**	**11:00 - 11:00**	**76**
		d	**17/07 - 18/07/2019**	**13:00 - 13:00**	**78**
7	Autumn 2019	*c*	14/10 - 15/10/2019	10:00 - 10:00	88
		d	15/10 - 16/10/2019	11:15 - 11:15	87
8	**Winter 2020**	***c***	**10/02 - 11/02/2020**	**09:00 - 09:00**	**107**
		d	**11/02 - 12/02/2020**	**10:15 - 10:15**	**108**

Table S2: Means, standard deviations (±) and ranges (min/max) of water temperature (T), salinity (S), oxygen concentration (O_2), turbidity (TU), partial pressure of CO_2 (pCO_2) and chlorophyll *a* concentration (Chl *a*) values during each 24-hour cycle at the seasonal and spatial scales.

		T (°C)	**S**	**O_2 ($mg.L^{-1}$)**	**TU (NTU)**	**pCO_2 (ppmv)**	**Chl *a* ($\mu g.L^{-1}$)**
Winter	*a*	**9.5 ± 0.3** (9.1/10.4)	**32.5 ± 0.2** (31.9/32.9)	**8.92 ± 0.25** (8.23/9.24)	**7.1 ± 7.3** (0.0/45.5)	**440 ± 25** (377/510)	-
	b	**9.8 ± 0.5** (8.9/11.3)	**31.0 ± 1.4** (27.5/32.5)	**8.63 ± 0.30** (8.05/9.84)	**13.8 ± 7.7** (4.1/56.9)	**550 ± 33** (337/518)	-
	c	**11.5 ± 0.7** (10.2/12.9)	**27.8 ± 0.7** (27.0/29.7)	**9.20 ± 0.70** (8.22/11.20)	**7.5 ± 4.3** (2.2/27.4)	**343 ± 87** (130/519)	**1.31 ± 0.27** (1.09/1.93)
	d	**10.2 ± 0.6** (9.2/11.1)	**21.4 ± 0.0** (21.3/21.5)	**10.06 ± 0.51** (9.48/11.00)	**1.4 ± 0.7** (0.7/6.2)	**347 ± 30** (302/438)	**3.42 ± 0.37** (2.66/3.77)
Spring	*a*	**15.0 ± 0.7** (14.1/16.5)	**31.5 ± 0.0** (31.4/31.5)	**8.51 ± 0.52** (7.10/9.13)	**4.7 ± 4.3** (0.1/27.6)	**390 ± 40** (342/505)	-
	b	**15.5 ± 0.9** (14.1/16.9)	**31.2 ± 0.3** (30.3/31.6)	**8.07 ± 0.65** (6.41 ± 8.94)	**13.4 ± 18.7** (3.1/8.9)	**443 ± 44** (371/551)	-
	c	**17.1 ± 1.8** (14.3/19.9)	**33.7 ± 0.2** (33.3/34.0)	**9.20 ± 2.51** (5.39/9.23)	**4.0 ± 2.7** (1.9/26.9)	**135 ± 165** (6/425)	**1.74 ± 0.08** (1.62/1.81)
	d	-	-	-	-	-	-
Summer	*a*	**22.9 ± 1.6** (21.0/26.9)	**34.2 ± 0.3** (33.6/34.9)	**7.98 ± 1.15** (4.91/9.81)	**2.4 ± 2.3** (0.0/10.1)	**385 ± 61** (267/522)	-
	b	**23.9 ± 1.3** (21.9/26.1)	**34.7 ± 0.5** (33.9/35.6)	**6.78 ± 1.08** (4.47/9.34)	**8.1 ± 4.5** (1.6/62.5)	**454 ± 55** (374/590)	-
	c	**23.5 ± 2.5** (20.1/28.4/	**38.8 ± 2.3** (33.5/42.6)	**6.62 ± 1.87** (2.46/10.70)	**4.0 ± 2.5** (1.1/14.0)	**242 ± 116** (25/430)	**5.21 ± 1.67** (3.37/7.62)
	d	**23.3 ± 1.6** (21.2/8.1)	**35.8 ± 1.5** (33.3/38.1)	**6.48 ± 2.25** (3.48/10.06)	**1.5 ± 0.6** (0.7/4.7)	**377 ± 85** (250/508)	**1.78 ± 0.27** (1.40/2.04)
Autumn	*a*	**10.9 ± 1.5** (17.6/22.0)	**35.2 ± 0.1** (35.1/35.7)	**8.56 ± 0.83** (6.55/10.35)	**1.4 ± 1.9** (0.1/12.4)	**460 ± 58** (334/569)	-
	b	**20.8 ± 1.2** (18.8/23.1)	**35.9 ± 0.5** (35.1/36.9)	**7.43 ± 0.97** (4.92/8.81)	**7.2 ± 6.3** (1.7/40.6)	**503 ± 46** (422/630)	-
	c	**17.1 ± 0.9** (15.1/18.5)	**35.0 ± 0.3** (34.6/36.7)	**6.22 ± 0.78** (4.87/7.58)	**5.2 ± 2.2** (2.4/16.0)	**622 ± 57** (522/721)	**13.72 ± 7.20** (4.3/23.1)
	d	**15.9 ± 0.4** (15.4/16.8)	**38.2 ± 0.1** (38.0/38.4)	**8.18 ± 1.28** (6.74/10.62)	**0.1 ± 0.1** (0.0/0.8)	**155 ± 30** (110/218)	**1.33 ± 0.37** (1.17/2.16)

Table S3: Means, standard deviations (±) and ranges (min/max) of wind speed ($km.h^{-1}$), k660 ($cm.h^{-1}$) and water-atmosphere CO_2 flux (FCO_2 in $mmol.m^2.h^{-1}$) values during each 24-hour cycle at the seasonal and spatial scales.

		Wind speed ($km.h^{-1}$)	**K660 ($cm.h^{-1}$)**	**FCO_2 ($mmol.m^2.h^{-1}$)**
Winter	*a*	**23 ± 7** (11/39)	**11.10 ± 7.20** (2.30/29.37)	**0.10 ± 0.08** (0.01/0.34)
	b	**17 ± 7** (7/30)	**6.78 ± 4.51** (0.93/17.39)	**0.15 ± 0.12** (0.02/0.41)
	c	**27 ± 5** (16/34)	**14.79 ± 5.29** (4.95/22.37)	**-0.14 ± 0.27** (-0.71/0.33)
	d	**15 ± 5** (4/24)	**4.78 ± 2.77** (0.37/10.43)	**-0.04 ± 0.04** (-0.14/0.04)
Spring	*a*	**20 ± 8** (4/33)	**10.80 ± 7.65** (0.35/24.76)	**-0.18 ± 0.18** (-0.56/0.00)
	b	**12 ± 4** (4/19)	**3.92 ± 2.51** (0.33/7.76)	**0.03 ± 0.05** (-0.08/0.13)
	c	**16 ± 6** (10/25)	**6.56 ± 4.46** (1.08/18.00)	**-0.19 ± 0.19** (-0.64/0.00)
	d	-	-	-
Summer	*a*	**15 ± 4** (6/24)	**6.75 ± 3.70** (0.98/14.12)	**-0.06 ± 0.16** (-0.34/0.19)
	b	**16 ± 6** (7/28)	**8.34 ± 5.52** (1.44/23.07)	**0.18 ± 0.18** (-0.03/0.61)
	c	**13 ± 4** (4/19)	**4.46 ± 2.49** (0.43/9.46)	**-0.04 ± 0.03** (-0.13/0.00)
	d	**15 ± 6** (2/23)	**7.12 ± 4.60** (0.11/14.77)	**-0.02 ± 0.04** (-0.09/0.06)
Autumn	*a*	**10 ± 5** (4/19)	**3.13 ± 2.13** (0.87/5.97)	**0.03 ± 0.07** (-0.11/0.14)
	b	**14 ± 6** (16/24)	**6.42 ± 6.98** (0.99/24.62)	**0.27 ± 0.40** (0.01/1.43)
	c	**35 ± 8** (20/48)	**27.69 ± 11.52** (9.01/48.78)	**0.51 ± 0.30** (0.15/1.17)
	d	**42 ± 7** (31/54)	**38.40 ± 12.85** (20.54/62.36)	**-0.77 ± 0.24** (-1.35/-0.41)

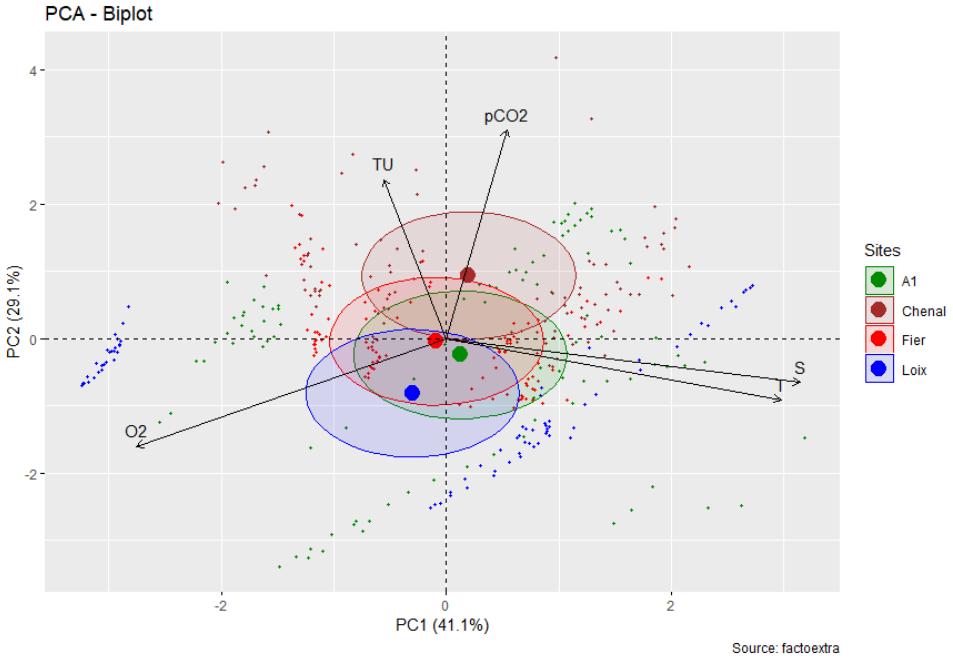

Annexe 4: Principal component analysis (PCA - biplot) at the spatial scales. Chl *a* concentrations are not shown because they were not studied for stations *a* and *b* (Fier d'Ars bay and Vieux Port channel respectively). The different ellipses represent the Euclidean distance with the "barycentre".

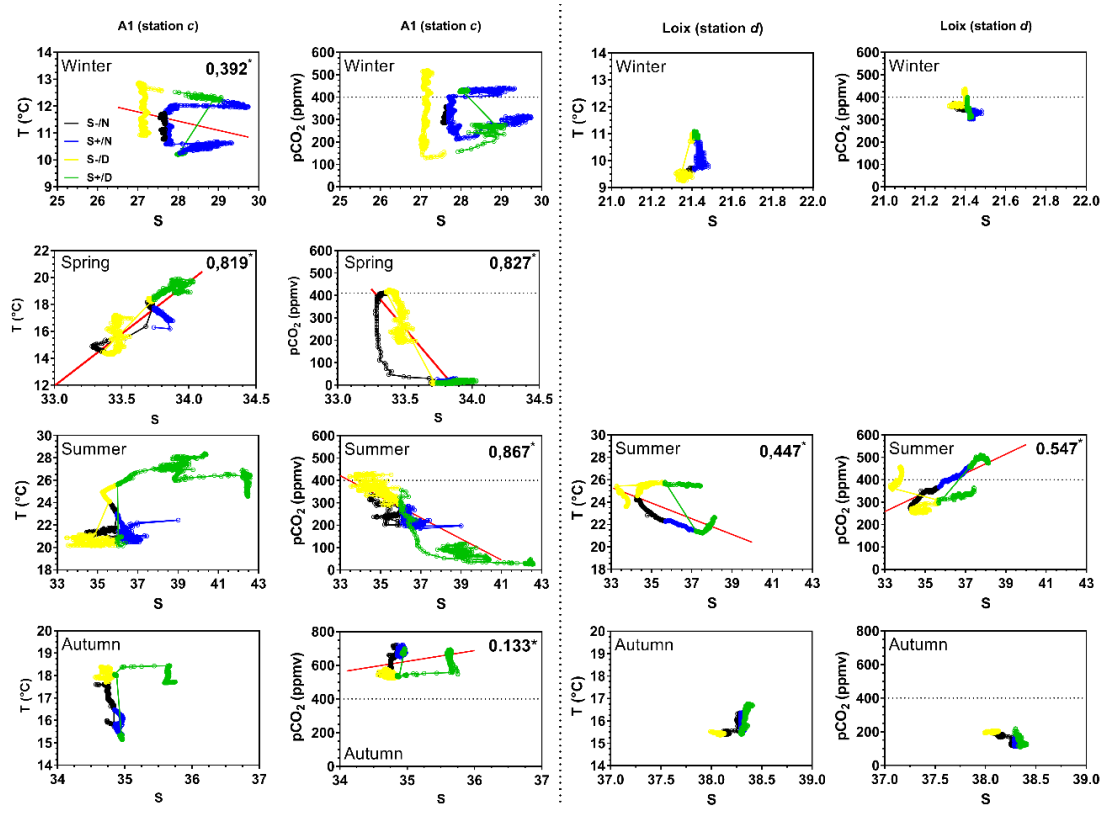

Annexe 5: T/S and pCO_2/S correlations at the diurnal, tidal and seasonal scales for the stations *c* and *d* (A1 and Loix salt marshes respectively). Very small R^2 are not represented. Periods of high and low salinity were distinguished using the Q_{50} (median) salinity for each 24-hour cycle. S+/D: strong salinity day; S-/D: weak salinity day; S+/N: strong salinity nigh; S-/N: weak salinity nigh.

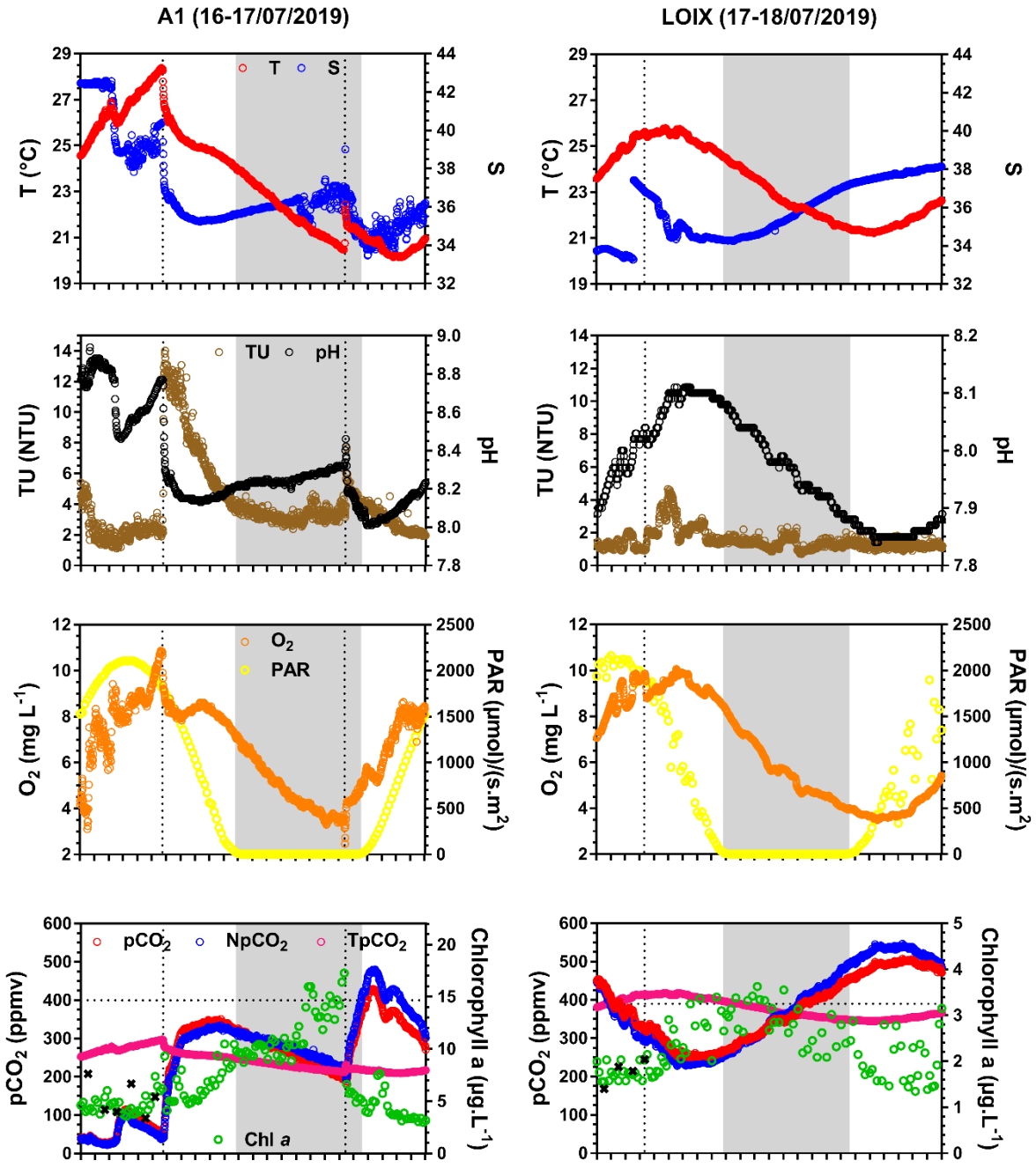

Annexe 6: Temporal variations of water temperature (T, °C), salinity (S), turbidity (TU, NTU), pH, oxygen concentration (O_2, mg.L^{-1}), photosynthetically active radiation (PAR, µmol.s^{-1}.m^{-2}), pCO_2, $NpCO_2$, $TpCO_2$ (ppmv) and chlorophyll *a* concentrations (Chl *a*, µg.L^{-1}) during a 24-hour cycle at stations *c* and *d* respectively (A1 and Loix salt marshes) in summer 2019. The Chl *a* scales are not the same between the two stations. The black crosses represent Chl *a* measured in the laboratory from water samples (*in vivo*). Grey areas correspond to the night period. The vertical dotted lines correspond to coastal water incoming into the marshes at each high tide. The horizontal dotted lines correspond to CO_2 atmospheric concentration determined by the EC station (station *e*, Figure 6). At station *c*, the Spearman correlation between pCO_2 and O_2 was -0.15 whereas the correlation between pCO_2 and marsh water height was +0.85 (curves not showed).

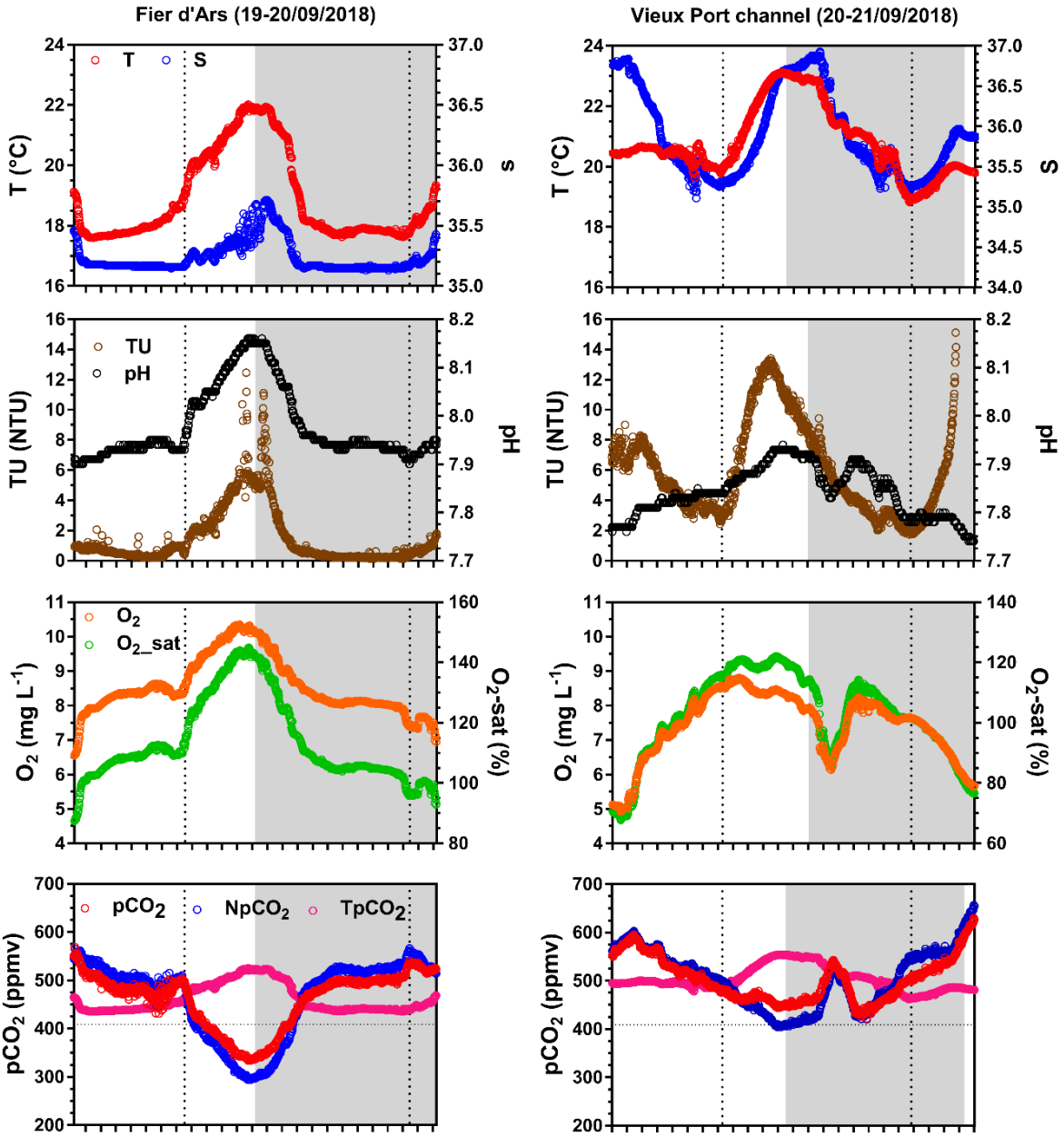

Annexe 7: Temporal variations of water temperature (T, °C), salinity (S), turbidity (TU, NTU), pH, oxygen concentration (O_2, $mg.L^{-1}$), oxygen saturation (O_2_sat, %), pCO_2, $NpCO_2$ and $TpCO_2$ (ppmv) during a 24-hour cycle at stations *a* and *b* respectively (Fier d'Ars and Vieux Port channel) in September 2018 (Autumn). Grey areas correspond to the night period. The vertical dotted lines correspond to horizontal advection of coastal waters at each high tide. The horizontal dotted lines correspond to CO_2 atmospheric concentration.

Abstract

Coastal environments such as the Charentais Sounds are key systems in the biogeochemical cycles coupling (C, N, P) between the land, the ocean and the atmosphere. Within the coastal zone, salt marshes are considered as CO_2 sinks associated to their significant autotrophic metabolism and sediment carbon (C) storage. However, this ecological functioning is more and more threatened by global change (acidification, sea level rise, eutrophication) and anthropogenic pressures decreasing blue C area potential worldwide. C dynamics over salt marshes are complex since various processes and fluxes take place at the different terrestrial-aquatic-atmospheric exchange interfaces at the spatio-temporal scales of the coastal zone. The ANR-PAMPAS research project allows a better understanding of marsh ecological functioning located in the Charentais Sounds according to their typology and management practices faced oceanic submersion risks. Related to the blue C sink ecological functioning, this internship specifically focused on the dynamic of water partial pressures of CO_2 (pCO_2) and associated relevant environmental parameters at diurnal, tidal and seasonal scales along a dyked salt marsh – channel – bay continuum within the Fier d'Ars coastal wetland (Ré Island). The diurnal/tidal measurements carried out from year 2018 to 2020 at stations along the continuum highlighted a strong biological control on water pCO_2 and associated metabolisms at diurnal and seasonal scales according to station typology and management practices too. During spring-summer seasons at dyked salt marsh stations, photosynthesis activity of macroalgae, seagrass and phytoplankton produced large CO_2 undersaturation. To the contrary during winter-autumn seasons, lower biological activity associated with microbial loop-type network particularly at channel water station induced large CO_2 oversaturation with regards to the atmosphere. Other non-temperature effect such as coastal water advection significantly influenced diurnal water CO_2 dynamics among connected stations. Over the year, the majority of the studied stations (bay and dyked marshes) behaved as CO_2 sinks (-0.03 ± 0.17 and -0.26 ± 0.38 $mmol.m^2.h^{-1}$ at Fier d'Ars Bay and Loix marsh respectively) while only the channel station connecting coastal waters of the bay to dyked marshes represented a CO_2 source to the atmosphere ($+0.16 \pm 0.24$ $mmol.m^2.h^{-1}$).

Key words: temperate salt marsh system, typology/management practice, water carbon dynamic, water-atmosphere CO_2 flux, biological pump, hydrodynamic advection, CO_2 source/sink.